JOURNAL OF PETROLOGY | VOLUME 52 | NUMBER 2 | PAGES 257–278 | 2011 | doi:10.1093/petrology/egq079

Along-Arc Variations in the Pre-Eruptive H_2O Contents of Mariana Arc Magmas Inferred from Fractionation Paths

S. W. PARMAN[1]*, T. L. GROVE[2], K. A. KELLEY[3] AND T. PLANK[4]

[1]DEPARTMENT OF EARTH SCIENCES, BROWN UNIVERSITY, PROVIDENCE, RI 02912, USA

[2]DEPARTMENT OF EARTH, ATMOSPHERIC AND PLANETARY SCIENCES, MASSACHUSETTS INSTITUTE OF TECHNOLOGY, CAMBRIDGE, MA 02139, USA

[3]GRADUATE SCHOOL OF OCEANOGRAPHY, UNIVERSITY OF RHODE ISLAND, NARRAGANSETT, RI 02882, USA

[4]DEPARTMENT OF EARTH SCIENCES, BOSTON UNIVERSITY, BOSTON, MA 02215, USA

RECEIVED DECEMBER 30, 2009; ACCEPTED NOVEMBER 8, 2010
ADVANCE ACCESS PUBLICATION DECEMBER 14, 2010

New experimental results are presented on the effects of dissolved H_2O during low-pressure (<2 kbar) crystal fractionation in Mariana Arc magmas. The resulting fractionation paths are used to infer the pre-eruptive H_2O concentrations of Mariana lavas from seamounts and islands. Estimated pre-eruptive H_2O concentrations for Mariana seamounts (2–3 wt %) are relatively constant and similar to three out of eight of the subaerial volcanoes (Alamagan, Pagan and Asuncion). These H_2O concentrations are also similar to measured H_2O concentrations in Mariana back-arc lavas. Lavas from the remaining islands (Guguan, Agrigan, Uracas, Anatahan and possibly Sarigan) have significantly higher H_2O (5–6%) than the other seamounts and islands. These high-H_2O islands are distributed throughout the arc and do not show any relation to variations in subduction parameters such as subduction angle or obliquity. Analysis of the H_2O concentrations of olivine-hosted melt inclusions from seven islands (Guguan, Pagan, Agrigan, Anatahan, Alamagan, Asuncion and Sarigan) and one seamount (Fukujin) match the estimates inferred from the liquid lines of descent. One interpretation of our results is that the flux of volatiles from the Mariana sub-arc mantle is fundamentally heterogeneous. Alternatively, the variations in pre-eruptive H_2O concentrations could reflect variations in the depth and extent of fractionation of Mariana magmas.

KEY WORDS: *experimental petrology; Mariana arc; H_2O; fractionation; andesite*

INTRODUCTION

Although H_2O plays a major role in magmatic processes at subduction zones, quantifying the pre-eruptive amount of H_2O dissolved in arc magmas is not straightforward. This is because the solubility of H_2O declines rapidly as magmas approach the surface (Dixon *et al.*, 1995), with the result that the lava flows generally degas most of their original H_2O contents. Thus the whole-rock concentration of H_2O in a lava sample is primarily a product of degassing processes and only distantly reflects the pre-eruptive H_2O content.

A number of indirect methods can be used to estimate the pre-eruptive H_2O concentrations of arc magmas. One approach is to use experimental phase equilibria data to infer the H_2O concentrations required for a magma to be in equilibrium with the mantle from which it was produced (Green & Ringwood, 1968; Kushiro, 1974; Tatsumi, 1981; Baker *et al.*, 1994; Gaetani & Grove, 1998). This method estimates the H_2O content of the parental melt, prior to crustal fractionation.

Similarly, experimental data can be used to estimate magmatic H_2O concentrations from the composition of glomerocrysts and phenocrysts found in the magmas (Baker & Eggler, 1987; Gaetani *et al.*, 1993; Sisson & Grove, 1993; Grove *et al.*, 2003). This yields the H_2O content of the magma during fractionation at low pressures.

*Corresponding author. Telephone: 1-401-863-3352. E-mail: stephen_parman@brown.edu

A somewhat more direct approach is to examine H_2O concentrations of melt inclusions (MI). These are small volumes of melt enclosed within crystals as they grew at depth, and so may potentially preserve undegassed volatile concentrations (Lee & Stern, 1998; Newman *et al.*, 2000; Danyushevsky *et al.*, 2002; Kent & Elliott, 2002; Wallace, 2005; Shaw *et al.*, 2008). However, diffusive re-equilibration between the MI and host magma can lead to post-entrapment modification of the H_2O concentrations (Portnyagin *et al.*, 2008). Despite the difficulties, these combined approaches have provided a wealth of data on the role of H_2O in arc magmatism and elemental inputs from the subducting slab (Tatsumi, 1981; Grove & Baker, 1984; Baker & Eggler, 1987; Gaetani *et al.*, 1993; Sisson & Grove, 1993; Baker *et al.*, 1994; Kawamoto, 1996; Newman *et al.*, 2000; Kent & Elliott, 2002; Grove *et al.*, 2003; Wallace, 2005; Di Carlo *et al.*, 2006; Wade *et al.*, 2006; Benjamin *et al.*, 2007; Hamada & Fujii, 2008).

Ideally, these methods could be used to measure how magmatic volatile concentrations vary along and across arcs. This would go a long way towards helping us understand the processes by which volatiles are transferred from the subducting lithosphere into the mantle and eventually to the surface. Does H_2O vary in response to changes in the dip or obliquity of subduction? With the age of the slab? Or the rate of convergence? Or is the volatile flux controlled by the type of sediment input? Here, several of the current techniques used to infer H_2O concentrations have a common weakness. They generally require samples that are difficult or impossible to find at most locations. The mantle equilibrium approach requires finding near-primary melts, which are rare (Tatsumi *et al.*, 1981, 1983; Grove *et al.*, 2003). The glomerocryst approach can be used only if there are glomerocrysts or inclusions. Although more common than near-primary melts, they are not ubiquitous. Likewise, well-preserved, glassy melt inclusions are not present in most samples. Thus producing continuous profiles of magmatic H_2O concentrations along or across arcs is challenging with these methods.

What is desirable is a method for inferring H_2O concentrations that does not require special or rare samples, and that can be applied to all (or nearly all) volcanoes. Although single, erupted lava samples do not record their pre-eruptive volatile contents, it may be that suites of related lavas do. As magmas crystallize at depth, their major and trace element (TE) compositions evolve along lines determined by their phase equilibria. These are the so-called liquid lines of descent (LLDs). If this fractionation takes place at depth where volatile solubility is relatively high, the LLD may record the pre-eruptive volatile concentration of the magma, as the stabilities of many minerals (particularly silicates) are highly sensitive to H_2O concentration (e.g. Housh & Luhr, 1991). Thus by quantifying the effects of H_2O on LLDs, one may be able to infer undegassed H_2O concentrations of magma suites from their LLDs, even though the magmas themselves degas before eruption. Because whole-rock major and trace element data are available for thousands of samples of arc volcanoes, this method offers the hope of producing estimates of pre-eruptive H_2O concentrations for enough volcanoes to examine along-arc volatile contents. As with melt inclusion and glomerocryst approaches, the LLD-based methods estimate H_2O contents of magmas during fractionation in the crust, not of the parental basaltic melts.

This is not a new idea or approach. The effect of H_2O on LLDs is well known (Woodhead, 1990; Gaetani *et al.*, 1993) and is fundamental to existing explanations for the difference between the calc-alkaline and tholeiitic differentiation trends (Miyashiro, 1974; Grove & Baker, 1984). However, a number of technical advancements make re-examination of such an approach timely. First, the number of hydrous experiments on arc magmas has increased as a result of improvements in experimental techniques (Sisson & Grove, 1993; Kawamoto, 1996; Gaetani & Grove, 1998; Di Carlo *et al.*, 2006; Pichavant & Macdonald, 2007; Hamada & Fujii, 2008). Second, techniques for analyzing the compositions of experiments, especially H_2O, have improved, allowing the composition of all phases in experiments to be determined. Finally, and perhaps most importantly, the database of arc magma compositions has grown exponentially. In particular, the rise of rapid inductively coupled plasma mass spectrometry analyses has produced a great increase in the amount of available trace element data, allowing the magmas to be screened for crystal accumulation effects. This is critical, as most (maybe all) magmas are affected to some extent by magma mixing and crystal accumulation effects. The TE data allow these effects to be minimized.

The model presented is based on similar data to those used in the models of Sisson & Grove (1993) and Pichavant & Macdonald (2007), but is different in its approach. Those studies used melts saturated in four or five phases to fit the melt compositions for H_2O content. Thus the H_2O content of single samples can be estimated using bulk compositions. In this study, the plag-in boundary is parameterized and pre-eruptive H_2O contents can be inferred only for suites of magmas where LLDs can be defined.

The goal of this work is to re-examine the utility of using LLDs to infer pre-eruptive magmatic volatile concentrations, with the ultimate aim of examining along-arc volatile variations and overall volatile cycling. We focus on the Mariana arc (Fig. 1) as it has one of the most comprehensive databases of lava compositions and, being an oceanic arc, the magmas are least affected by crustal contamination. Also, because of the number of dredging

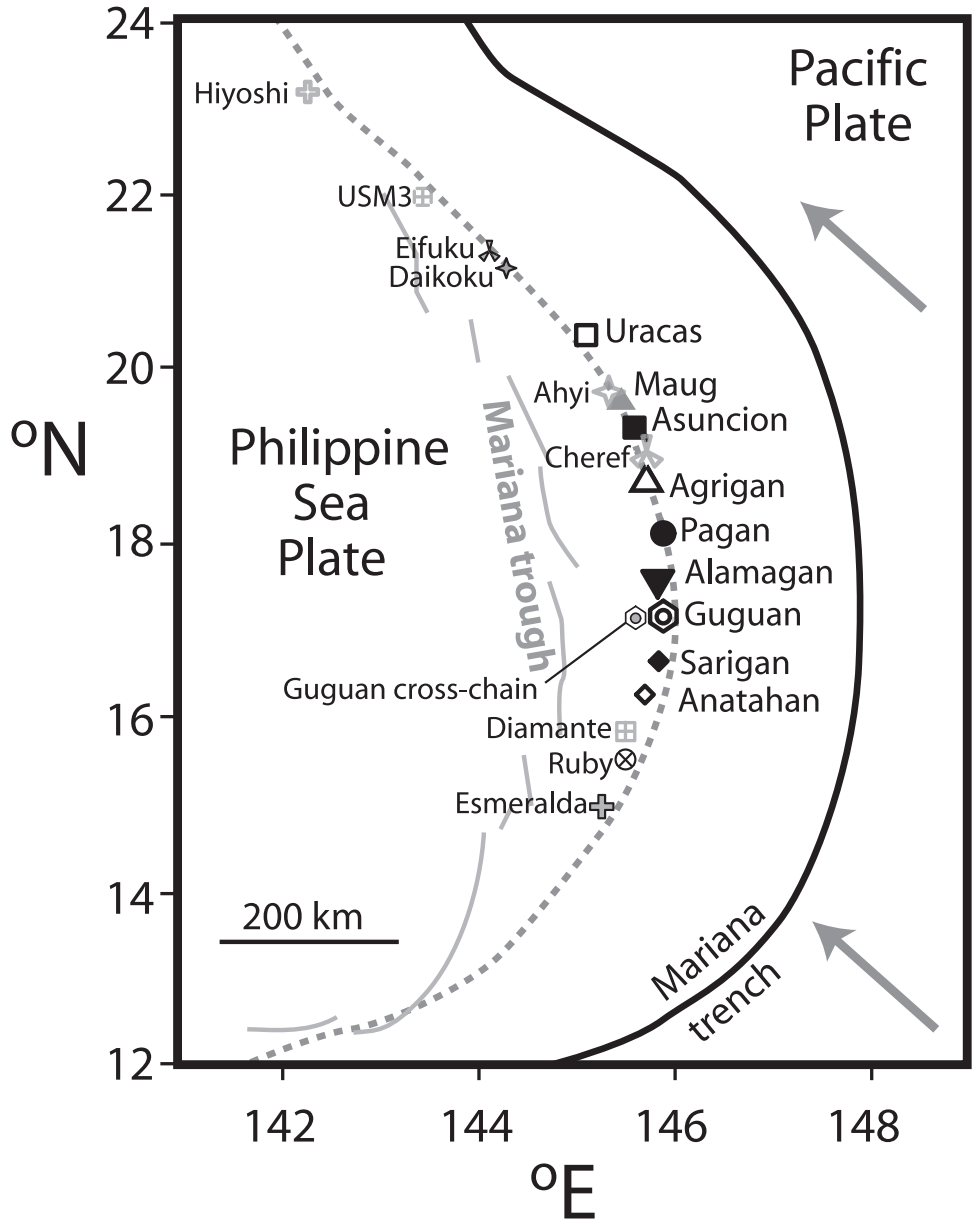

Fig. 1. Map showing the locations of samples used in this study from volcanoes and seamounts in the Mariana arc (after Pearce *et al.*, 2005, fig. 1). Symbols are those used in Figs 4–9. Also shown are the location of the trench (bold black line), the back-arc spreading segments in the Mariana Trough (fine black lines), the location of the subducting slab at a depth of 100 km (dashed line) and the direction of Pacific plate motion (gray arrows).

cruises in the area, both islands and seamounts can be compared.

We present new experimental results and show that Mariana LLDs do appear to record pre-degassing H_2O contents. In particular, the maximum Al_2O_3 reached by an LLD correlates well with dissolved H_2O concentration. By identifying the maximum Al_2O_3 in related natural samples (screened for plagioclase accumulation), estimates of the pre-eruption H_2O concentrations can be made. Some of the LLDs appear to require up to 6 wt % H_2O in magmas at the time of plagioclase saturation. We compare our results with melt inclusion (MI) data from the same volcanoes and show that the two methods yield consistent results. At this point, the main source of error on the H_2O estimates is not the experiments, but in identifying tight LLDs in the magma suites. In part, this is simply a fact of nature. An LLD is a theoretical concept that assumes a perfectly closed magmatic system. Nature

is not so kind. Magma mixing and crystal accumulation are ubiquitous in arc magmas and pure LLDs probably do not exist. However, the TE allow the effects of these processes to be minimized and chemical trends that approach LLDs to be delineated. Thus our study suggests that detailed petrographic and geochemical studies of the magmatic suites to define well-constrained LLDs could allow significant advances in our understanding of the H_2O contents of arc magmas and volatile fluxes at arcs. Where present, melt inclusions provide better constraints on pre-eruptive volatile concentrations than the LLD method at this point. However, when suitable glassy melt inclusions cannot be found, the LLD method does allow some constraint to be placed on pre-eruptive volatile contents.

MARIANA GEOLOGY AND GEOCHEMISTRY

The Mariana arc lies in the western Pacific Ocean, and is produced by the subduction of the Pacific plate under the Philippine Sea plate (see review by Stern *et al.*, 2003). Because of the curvature of the arc, the obliquity of subduction varies from nearly orthogonal in the south to nearly parallel in the north (Fig. 1). Volcanism extends from 13°N to *c.* 24°N, depending on where one places the boundary between the northern Mariana and southern Izu arc. It is generally divided into three main regions, the central island province (CIP), encompassing all nine of the subaerial volcanoes along with a number of seamounts, and the northern and southern seamount provinces (NSP and SSP), which as their names indicate, contain only seamounts (Stern *et al.*, 2003).

Mariana magma compositions span the calc-alkaline to tholeiitic divide, and are fairly mafic for arc magmas (Woodhead, 1988; Bloomer *et al.*, 1989; Meen *et al.*, 1998; Stern *et al.*, 2003), although an important minority of silicic and alkaline magmas are present as well (Wade *et al.*, 2005). Al_2O_3 concentrations can be high (over 20 wt %) even in mafic magmas. Some have argued that this is due to high H_2O concentrations and the suppression of plagioclase nucleation, leading to Al_2O_3 increase during ol–cpx only fractionation (Woodhead, 1988). Others have argued that the high Al_2O_3 concentrations are due to plagioclase addition, pointing out that the lavas are phenocryst-rich, and often display signs of magma mixing (Lee & Stern, 1998; Meen *et al.*, 1998). Likewise, FeO concentrations have a range of values. Most follow a tholeiitic, FeO-enrichment trend, but a few do not, and these more closely resemble calc-alkaline magmas. Given the complexity of the data and the diversity of viewpoints about their origin, it is not surprising that estimates of pre-eruptive H_2O concentrations in the Mariana arc span a fairly large range (1–6%; Tatsumi *et al.*, 1983; Newman *et al.*, 2000; Shaw *et al.*, 2008; Kelley *et al.*, 2010).

EXPERIMENTAL METHODS

The concept behind the experimental study is to quantify the delay in plagioclase saturation over a range of bulk compositions, including H_2O concentrations. Although the experiments are similar to natural LLDs, there are important differences. In particular, H_2O fugacity is fairly constant along the experimental LLDs because all of the experiments are H_2O-saturated. In nature H_2O probably changes continuously along an LLD, rising as a result of fractionation and falling as a result of degassing. Thus the purpose of the experiments is not to perfectly mimic natural LLDs, but to find the plag-in point over a range of conditions and compositions. Also, we assume that the main effect on the plag-in boundary is due to the H_2O fugacity (P_{H2O}), such that the same magmatic H_2O content at different pressures would have a similar effect on the plag-in boundary.

Two compositions were chosen for the experiments, one from the island of Pagan (PAF3b from Woodhead, 1989) and one from Sarigan (SA-61–2 from Meijer & Reagan, 1981). The primary criteria for choosing these compositions were their high MgO concentration and Mg-number [Mg-number = MgO/(MgO + FeO), oxides in moles] and their spread in major element composition, covering much of the range of Mariana lavas. Synthetic versions of these compositions were made by mixing high-purity oxides. The FeO concentrations of the original mixes (PAF1 and SAR1) were too low (because of a calculation error), so new mixes with the correct FeO were made (PAF2 and SAR2). Despite their low FeO, the experiments on PAF1 and SAR1 are reported, as they provide useful information on phase equilibria and the effects of FeO on the LLDs. The compositions of all starting materials are given in Table 1.

The experiments were run in a rapid-quench, externally heated gas-pressure vessel (EHPV; made of zirconium–hafnium–molybdenum). A multiple-capsule technique similar to that of Sisson & Grove (1993) was used. The starting compositions were loaded into Au capsules for runs below 1050°C and into $Au_{90}Pd_{10}$ capsules for higher temperature runs. One end of the sample capsule was welded shut, whereas the other was merely crimped closed to provide a pathway for H_2O. This sample capsule was placed inside a larger, thicker $Au_{80}Pd_{20}$ capsule along with 20 μl of purified H_2O (syringed into the bottom of the capsule). Within the outer capsule, two Pt capsules were placed above the sample capsule. These contained mixtures of Ni and NiO to provide an oxygen buffer. As with the sample capsule, the tops of these capsules were not welded to allow fluid exchange. Nickel concentrations in experimental olivines and melts are all below

Table 1: Experimental starting compositions (wt %)

	PAF1	PAF2	SAR1	SAR2
SiO_2	50·14	49·74	53·21	51·88
TiO_2	0·65	0·66	0·71	0·72
Al_2O_3	17·32	17·13	16·18	15·68
Cr_2O_3	0·03	0·02	0·00	0·02
FeO	9·46	10·35	7·77	8·93
MnO	0·20	0·21	0·16	0·16
MgO	7·36	7·34	7·75	7·55
CaO	12·37	11·97	11·83	11·60
Na_2O	1·40	1·40	1·15	2·00
K_2O	0·40	0·49	0·43	0·55
P_2O_5	0·06	0·10	0·05	0·10
NiO	0·00	0·00	0·00	0·00
Total	100·0	100·0	100·0	100·0

0·05 wt %, indicating that Ni from the buffers did not contaminate the sample capsule. Finally, both ends of the outer capsule were welded shut to prevent H_2O loss.

The multiple-capsule assembly was placed in the EHPV and pressurized with Ar and a small amount of methane (<1% by volume). The methane breaks down at high temperature and provides a small hydrogen partial pressure that limits loss of H_2 owing to diffusion. The samples were first pressurized and then placed in the vertical tube furnace, which was standing at 900°C. Once in the furnace, the temperature was ramped up to the run temperature at *c.* 6°C/min. Most run durations were between 20 and 28 h. From experience, this run duration is long enough to allow the minerals and melts to approach equilibrium, but short enough to prevent the experiment from drying out. One experiment (PAF7) was run for 3 h to show the effects of disequilibrium (Table 2), but otherwise is not used in the discussion.

Experiments were run over a range of temperatures and pressures to delineate the phase assemblages. Run conditions for all experiments are given in Table 2 and all phase compositions are given in Table 3. Most experiments were performed at 2 kbar, although three lower pressure experiments were also performed. After the experiments, the capsule was checked for the presence of free water. Only experiments with free water are reported. Also, the buffer capsules were checked for the presence of both Ni and NiO and only experiments with both are reported. In addition to the hydrous experiments, two anhydrous experiments were performed at 1 atm in a gas-mixing furnace. Although not at high pressure these should approximate the dry fractionation path at 2 kbar, as the effect of pressure on the phase equilibria is small compared with the effect of H_2O (Grove *et al.*, 1992). For all experiments, the phases present were mass-balanced with the starting composition to check for chemical interaction with the capsule, Fe loss in particular. Experiments with high residuals and/or high Fe loss were rejected and are not reported. Disequilibrium in the 3 h experiment (PAF7) produces high residuals in the mass balance owing to the heterogeneity of the solid phases. In addition, mineral–melt exchange K_D values were used to check for an approach to equilibrium, by comparison with previous studies (Housh & Luhr, 1991; Sisson & Grove, 1993; Grove *et al.*, 2003). In general, experiments that failed to attain equilibrium, had dried out or had lost Fe to the capsule are easily identifiable using mass balance and K_D values. Only experiments that passed all tests are reported in Tables 2 and 3 (with the exception of PAF7) and used in the following analysis.

All experiments were analyzed with a JEOL733 Superprobe at MIT (Table 3). Run conditions and data reduction methods are the same as those of Grove *et al.* (2003). Water concentrations in the experimental glasses were calculated by a combination of ion probe and electron probe data. Estimating H_2O concentrations by summation deficit (H_2O_{SD}) of the microprobe data is convenient, but overestimates the real H_2O concentrations. To correct for this, we adopt the method used by Pichavant & Macdonald (2007) and calibrate the summation deficit H_2O estimate to secondary ion mass spectrometry (SIMS) analyses of H_2O in a few experimental melts. Three experimental glasses were analyzed for H_2O by ion probe. [See Medard & Grove (2008) for analytical conditions.] This yields the relationship for the ion probe corrected H_2O concentrations: $H_2O_c = 0{\cdot}73\,H_2O_{SD}$. Further details about water concentrations are given in the online Supplementary Material (online Fig. 1 and Table 2, available at http://www.petrology.oxfordjournals.org). Spinels in the experiments were micron-sized and were too small to analyze with the microprobe, with one exception (PAF25).

EXPERIMENTAL RESULTS

The crystallization sequence for each composition is shown in Fig. 2. The main difference between the PAF and SAR composition is the late appearance of plagioclase (relative to ol and cpx) in SAR. This is consistent with the low bulk Al_2O_3 concentration in SAR. Although the near-liquidus phase relations are not well defined, on the basis of the phase fractions it appears that ol crystallizes just before cpx in PAF, but the reverse is true for SAR.

The isothermal equilibrium crystallization paths produced by the experiments are shown in Fig. 3. It should be noted that all analyses of hydrous experimental glasses are presented in the figures on an anhydrous basis for comparison with the Mariana lavas. All elements show good

Table 2: Experimental results

Run no.	*P* (GPa)	*T* (°C)	Exp. comp.	Time (h)	cap.	gl	ol	cpx	plag	spin	ΣR^2	ol K_D^{Fe-Mg}	cpx K_D^{Fe-Mg}	plag K_D^{Ca-Na}
PAF1 hydrous experiments														
PAF6	0·20	1060	PAF1	24	Au	0·893(24)*	trace	0·093(25)	—	0·015(6)†	0·300	0·254	0·605	—
PAF22	0·20	1050	PAF3	28	Au	0·877(11)	0·024(3)	0·068(6)	0·031(6)	—	0·042	0·276	0·292	3·85
PAF5	0·20	1040	PAF1	24	Au	0·872(32)	0·025(10)	0·072(18)	0·030(18)	—	0·375	0·270	0·257	3·89
PAF11	0·20	1037	PAF1	24	Au	0·794(28)	0·049(9)	0·069(16)	0·088(17)	—	0·280	0·283	0·263	2·67
PAF8	0·20	1030	PAF1	24	Au	0·768(23)	0·048(8)	0·100(14)	0·084(14)	—	0·205	0·302	0·285	3·23
PAF7	0·20	1040	PAF1	3	Au	0·932(40)	0·043(15)	—	trace	t.s.	0·958	0·322	—	2·72
PAF19	0·10	1050	PAF1	15	90–10	0·605(6)	0·071(2)	0·108(4)	0·215(4)	—	0·022	0·250	0·205	2·78
PAF20	0·10	1030	PAF1	9	90–10	0·530(10)	0·092(4)	0·148(6)	0·252(6)	—	0·042	0·307	0·235	2·09
PAF2 hydrous experiments														
PAF25	0·20	1090	PAF2	24	90–10	0·992(8)	—	—	—	trace	—	—	—	—
PAF24	0·20	1070	PAF2	20	90–10	0·987(7)	0·013(6)	—	—	t.s.	0·410	0·282	—	—
PAF16	0·20	1040	PAF2	24	Au	0·946(13)	0·025(7)	0·024(16)	0·005(5)	—	0·200	0·286	0·292	3·43
PAF17	0·20	1020	PAF2	24	Au	0·682(11)	0·072(4)	0·102(7)	0·144(7)	—	0·057	0·290	0·226	3·82
PAF15	0·16	1040?	PAF2	28	Au	0·758(10)	0·060(3)	0·069(6)	0·112(6)	t.s.	0·042	0·275	0·255	2·83
PAF2 anhydrous experiments														
PAF32	0·0001	1220	PAF2	70	loop	0·963(14)	—	—	0·034(13)	t.s.	0·511	—	—	1·73
PAF35	0·0001	1200	PAF2	140	loop	0·896(12)	—	—	0·102(12)	—	0·460	—	—	1·58
SAR1 hydrous experiments														
SAR9	0·20	1090	SAR	6	90–10	0·991(18)	0·012(9)	trace	—	—	0·522	0·286	0·255	—
SAR7	0·20	1070	SAR	22	90–10	0·921(10)	0·015(5)	0·064(10)	—	—	0·169	0·265	0·251	—
SAR5	0·20	1050	SAR	24·5	Au	0·867(7)	0·022(4)	0·112(8)	—	—	0·103	0·265	0·243	—
SAR3	0·20	1040	SAR	25	Au	0·833(8)	0·026(3)	0·137(5)	trace	—	0·030	0·268	0·251	4·40
SAR4	0·20	1030	SAR	24	Au	0·74(10)	0·041(5)	0·156(8)	0·064(9)	—	0·104	0·268	0·198	4·27
SAR2	0·20	1011	SAR	21	Au	0·621(14)	0·06(6)	0·195(9)	0·124(9)	—	0·131	0·311	0·192	6·12
SAR2 hydrous experiments														
SAR17	0·20	1070	SAR2	9·5	90–10	0·898(16)	0·023(8)	0·079(17)	—	—	0·410	0·271	0·253	—
SAR15	0·20	1060	SAR2	24	Au	0·890(12)	0·031(7)	0·079(13)	—	—	0·284	0·282	0·234	—
SAR11	0·20	1050	SAR2	22	Au	0·807(9)	0·043(5)	0·150(10)	—	—	0·136	0·213	0·244	—
SAR16	0·20	1040	SAR2	22·5	Au	0·793(16)	0·042(6)	0·132(10)	0·033(10)	—	0·125	0·287	0·241	4·57

Column headings: run number, pressure, temperature, experimental starting composition, experimental duration, capsule composition (Au or $Au_{90}Pd_{10}$), glass (mass fraction determined by mass balance), olivine, clinopyroxene, plagioclase, spinel, sum squared of residuals of mass balance, olivine Fe–Mg exchange K_D, clinopyroxene Fe–Mg exchange K_D, plagioclase Ca–Na exchange K_D.
trace, phase is present and was analyzed but error on mass balance was larger that mass fraction; t.s., too small to analyze with electron microprobe.
*Errors are given in parentheses, so 0·893(24) should be read as $0{\cdot}893 \pm 0{\cdot}024$.
†Because of thermostat failure during the experiment, the temperature was esimated. Spinels were present but too small to analyze. Spinel analyses from PAF25 or HJ1 were used for mass balance.

systematics and are consistent with the crystallization sequences. As discussed by Grove *et al.* (1997) there is not a significant difference between major element variation in a fractional crystallization path and the liquid line of descent defined by isothermal experiments when the amount of crystallization is <50 wt %. Thus, the crystallization paths defined by the experiments are considered to be a reasonable approximation to a fractional crystallization path. For the 2 kbar, H_2O-saturated experiments, SiO_2, TiO_2 and Na_2O rise steadily with fractionation. FeO rises slightly or is flat. CaO falls, although there may be a slight rise just below the liquidus of PAF2, owing to a small amount of ol-only crystallization before cpx appears.

Al_2O_3 rises at first and then falls dramatically. This is due to the onset of plagioclase crystallization, and it is this saturation boundary, and specifically the effect water

Table 3: Experimental run products

Run	Phase	*n*	SiO_2	TiO_2	Al_2O_3	Cr_2O_3	FeO	MnO	MgO	CaO	Na_2O	K_2O	P_2O_5	H_2O*	Total
PAF5	glass	20	47·85(22)	0·71(6)	17·17(14)	0·01(2)	8·69(19)	0·21(3)	5·58(11)	10·70(18)	1·28(15)	0·38(3)	0·05(4)	5·37(68)	97·69(40)
	ol	6	38·77(17)	0·01(1)	0·11(10)	0·00(0)	17·80(33)	0·35(2)	42·28(37)	0·41(8)	—	—	—	—	99·72(47)
	cpx	4	50·93(36)	0·38(3)	4·32(45)	0·53(12)	6·17(60)	0·19(2)	15·41(17)	21·92(37)	0·11(5)	—	—	—	99·97(9)
	plag	5	44·71(27)	—	36·03(19)	—	0·67(7)	—	0·12(2)	18·21(18)	0·56(6)	0·02(1)	—	—	100·31(16)
PAF6	glass	9	47·15(22)	0·63(7)	16·53(12)	0·00(0)	8·13(22)	0·18(2)	6·83(7)	11·54(8)	1·30(8)	0·36(1)	0·07(4)	5·31(32)	97·12(37)
	ol	6	39·26(16)	0·00(0)	0·04(2)	0·00(0)	14·21(52)	0·30(2)	45·18(34)	0·35(2)	—	—	—	—	99·34(42)
	cpx	1	46·73(–)	0·62(–)	10·76(–)	0·12(–)	8·60(–)	0·15(–)	11·47(–)	20·29(–)	0·42(–)	—	—	—	99·15(–)
PAF7	glass	13	47·90(19)	0·73(6)	17·07(20)	0·00(0)	8·80(21)	0·20(3)	5·53(18)	11·15(21)	1·34(10)	0·41(2)	0·07(2)	4·96(40)	99·77(57)
	ol	5	38·10(14)	0·09(1)	0·43(33)	0·07(1)	20·08(51)	0·39(2)	39·29(59)	0·62(16)	—	—	—	—	99·10(34)
	plag	4	45·64(20)	—	34·10(56)	—	1·05(20)	—	0·44(19)	18·54(30)	0·82(5)	0·03(0)	—	—	100·61(48)
PAF8	glass	7	48·41(17)	0·79(9)	16·98(19)	0·00(0)	8·89(37)	0·20(3)	4·93(42)	10·28(39)	1·52(7)	0·46(2)	0·09(3)	5·43(43)	99·18(82)
	ol	5	37·77(17)	0·08(1)	0·08(2)	0·07(1)	21·29(15)	0·46(3)	39·15(8)	0·40(3)	—	—	—	—	99·32(14)
	cpx	4	50·52(33)	0·51(6)	4·65(80)	0·30(7)	7·39(53)	0·17(4)	14·38(50)	21·07(35)	0·19(8)	—	—	—	99·20(56)
	plag	3	45·21(14)	—	35·04(28)	—	0·85(7)	—	0·16(3)	18·61(28)	0·85(16)	0·03(0)	—	—	100·76(21)
PAF11	glass	25	48·64(16)	0·76(7)	16·67(33)	0·01(1)	8·92(28)	0·19(2)	5·13(25)	10·61(28)	1·30(13)	0·41(2)	0·09(2)	5·29(52)	99·79(55)
	ol	6	38·99(27)	0·03(1)	0·08(6)	0·02(1)	20·08(27)	0·36(4)	40·80(56)	0·42(10)	—	—	—	—	100·78(39)
	cpx	5	51·75(49)	0·39(9)	3·38(43)	0·22(14)	6·89(29)	0·20(3)	15·06(53)	22·22(50)	0·17(8)	—	—	—	100·27(42)
	plag	7	45·59(51)	—	34·74(49)	—	0·88(8)	—	0·25(9)	18·39(25)	0·84(14)	0·03(0)	—	—	100·72(29)
PAF15	glass	13	49·04(33)	0·57(7)	16·33(32)	0·00(0)	10·45(26)	0·24(2)	4·93(30)	10·47(38)	1·35(10)	0·48(2)	0·13(5)	4·38(57)	99·65(49)
	ol	5	38·09(21)	0·04(8)	0·10(11)	0·04(2)	22·60(44)	0·39(2)	38·80(34)	0·37(2)	—	—	—	—	100·44(47)
	cpx	6	51·18(91)	0·40(10)	3·84(120)	0·32(11)	7·86(36)	0·18(4)	14·55(61)	21·61(42)	0·16(8)	—	—	—	100·11(38)
	plag	5	45·29(35)	—	34·71(23)	—	0·97(6)	—	0·19(6)	18·37(32)	0·84(16)	0·03(0)	—	—	100·41(14)
PAF16	glass	10	47·03(13)	0·65(7)	16·84(13)	0·00(0)	9·99(11)	0·23(7)	5·74(6)	11·39(15)	1·28(10)	0·40(2)	0·14(4)	4·71(33)	97·68(30)
	ol	6	38·58(14)	0·02(2)	0·11(9)	0·03(1)	20·07(41)	0·31(3)	40·40(34)	0·39(4)	—	—	—	—	99·91(27)
	cpx	5	50·29(55)	0·44(3)	4·65(68)	0·49(11)	7·40(99)	0·20(5)	14·55(41)	21·32(48)	0·18(4)	—	—	—	99·51(66)
	plag	8	44·48(32)	—	34·97(41)	—	0·80(3)	—	0·12(2)	18·66(29)	0·61(13)	0·02(1)	—	—	99·68(54)
PAF17	glass	11	49·02(24)	0·76(9)	16·35(26)	0·00(0)	10·41(28)	0·23(2)	4·31(20)	9·65(18)	1·35(10)	0·49(2)	0·12(3)	5·46(28)	99·29(35)
	ol	6	37·89(26)	0·05(1)	0·10(6)	0·03(1)	25·37(55)	0·39(5)	36·15(26)	0·45(1)					100·47(75)
	cpx	8	51·76(91)	0·39(11)	3·42(100)	0·27(9)	8·10(51)	0·23(3)	14·80(61)	21·38(46)	0·16(8)	—	—	—	100·51(69)
	plag	10	45·35(35)	—	34·75(115)	—	1·02(27)	—	0·35(44)	18·67(34)	0·68(11)	0·03(1)	—	—	100·86(44)
PAF19	glass	6	50·56(20)	0·93(6)	15·04(34)	0·02(2)	10·70(14)	0·23(3)	4·52(21)	9·52(30)	1·47(4)	0·54(3)	0·17(4)	4·58(62)	97·75(72)
	ol	5	37·88(20)	0·03(1)	0·19(17)	0·02(0)	22·50(34)	0·42(2)	38·09(41)	0·50(9)	—	—	—	—	99·66(59)
	cpx	5	52·05(52)	0·38(6)	2·80(44)	0·32(5)	7·54(59)	0·26(4)	15·53(54)	20·79(28)	0·28(6)	—	—	—	99·96(56)
	plag	5	45·59(16)	—	34·38(24)	—	0·86(4)	—	0·18(4)	18·12(10)	1·01(8)	0·04(1)	—	—	100·18(14)
PAF20	glass	6	51·29(39)	1·06(11)	16·02(114)	0·02(1)	9·73(54)	0·19(2)	3·73(36)	9·40(65)	1·53(17)	0·60(4)	0·16(3)	4·56(74)	98·94(89)
	ol	4	37·45(23)	0·05(2)	0·11(8)	0·02(0)	27·44(26)	0·49(3)	34·27(27)	0·47(8)	—	—	—	—	100·33(66)
	cpx	6	52·17(45)	0·41(6)	2·64(31)	0·22(8)	9·28(51)	0·30(3)	15·14(41)	19·67(56)	0·22(10)	—	—	—	100·03(38)
	plag	7	46·92(61)	—	33·39(53)	—	1·04(26)	—	0·31(18)	17·15(33)	1·34(15)	0·06(1)	—	—	100·21(52)
PAF22	glass	5	47·90(7)	0·72(5)	17·11(5)	0·00(0)	9·03(14)	0·21(1)	5·72(7)	10·97(9)	1·38(7)	0·40(1)	0·05(3)	4·74(15)	99·02(21)
	ol	6	39·27(25)	0·01(1)	0·09(12)	0·01(1)	18·34(28)	0·32(3)	42·13(38)	0·37(7)	—	—	—	—	100·54(38)
	cpx	8	50·61(74)	0·48(9)	5·34(122)	0·47(10)	6·74(77)	0·17(4)	14·63(56)	21·81(50)	0·12(5)	—	—	—	100·39(38)
	plag	6	45·04(35)	—	35·53(61)	—	0·86(12)	—	0·18(10)	18·79(26)	0·61(11)	0·03(1)	—	—	101·05(39)
PAF24	glass	5	46·24(13)	0·62(5)	16·69(11)	0·05(2)	9·57(9)	0·20(2)	6·57(4)	11·43(7)	1·22(11)	0·38(1)	0·04(1)	5·06(17)	99·657(23)
	ol	6	39·37(23)	0·02(1)	0·06(7)	0·01(1)	17·63(26)	0·31(2)	42·86(8)	0·36(1)	—	—	—	—	100·65(30)
PAF25	glass	5	45·81(12)	0·59(8)	16·87(4)	0·03(3)	9·88(6)	0·19(3)	6·94(4)	11·40(6)	1·29(7)	0·39(1)	0·21(23)	4·63(18)	100·32(22)
	sp	6	0·15(5)	0·44(4)	24·07(76)	28·73(71)	30·40(128)	0·28(2)	11·89(26)	0·35(2)	—	—	—	—	96·52(56)

(continued)

Table 3: Continued

Run	Phase	*n*	SiO_2	TiO_2	Al_2O_3	Cr_2O_3	FeO	MnO	MgO	CaO	Na_2O	K_2O	P_2O_5	H_2O*	Total
PAF29	glass	10	46·92(23)	0·66(5)	17·32(14)	0·02(1)	9·17(21)	0·23(2)	5·69(32)	11·56(14)	1·19(5)	0·38(1)	0·03(3)	4·96(25)	101·06(26)
	ol	6	39·21(39)	0·04(2)	0·24(13)	0·04(2)	18·76(39)	0·33(3)	41·02(37)	0·57(24)	—	—	—	—	100·24(56)
PAF32	glass	11	49·91(14)	0·69(3)	16·97(10)	0·03(2)	11·28(19)	0·21(2)	7·46(9)	11·56(11)	1·17(5)	0·32(1)	0·06(7)	—	99·67(26)
	plag	6	45·91(41)	—	33·47(39)	—	1·04(15)	—	0·45(10)	17·76(25)	1·04(14)	0·06(1)	—	—	99·72(39)
PAF35	glass	8	50·26(22)	0·70(8)	15·56(10)	0·05(3)	11·83(10)	0·18(3)	7·87(7)	10·83(7)	1·04(9)	0·36(1)	0·07(4)	—	98·78(29)
	plag	8	46·20(66)	—	34·00(50)	—	0·88(8)	—	0·37(9)	17·76(42)	1·07(14)	0·05(1)	—	—	100·33(35)
SAR2	gl	8	53·08(38)	1·04(9)	17·17(20)	0·04(2)	7·17(33)	0·16(2)	3·52(8)	7·74(17)	2·91(30)	0·75(2)	0·12(2)	4·82(26)	100·55(31)
	ol	5	38·41(25)	0·02(1)	0·02(2)	0·00(0)	23·66(29)	0·35(1)	37·45(36)	0·33(5)	—	—	—	—	100·24(25)
	cpx	5	52·27(32)	0·46(6)	2·86(38)	0·07(1)	6·26(72)	0·16(3)	16·00(29)	21·60(49)	0·19(8)	—	—	—	99·88(30)
	plag	6	46·25(27)	—	35·11(11)	—	0·65(3)	—	0·11(2)	17·86(27)	1·10(13)	0·03(1)	—	—	101·12(34)
SAR3	glass	8	50·45(54)	0·72(6)	17·80(17)	0·00(1)	7·14(19)	0·15(3)	4·85(26)	9·67(18)	1·99(35)	0·47(2)	0·07(3)	4·86(22)	100·52(45)
	ol	6	39·68(20)	0·02(1)	0·08(8)	0·00(1)	17·01(16)	0·26(1)	43·01(40)	0·35(9)	—	—	—	—	100·41(27)
	cpx	4	52·93(89)	0·55(31)	2·82(78)	0·07(1)	5·93(74)	0·17(4)	16·01(60)	22·13(16)	0·19(14)	—	—	—	100·79(21)
	plag	8	45·06(37)	—	35·04(26)	—	0·60(5)	—	0·14(6)	18·58(31)	0·87(12)	0·02(0)	—	—	100·31(41)
SAR4	glass	9	51·52(30)	0·78(6)	17·39(22)	0·00(1)	7·37(21)	0·15(2)	4·30(18)	8·97(20)	2·32(14)	0·53(2)	0·09(3)	4·78(24)	100·55(25)
	ol	5	38·87(14)	0·04(2)	0·06(4)	0·00(0)	18·99(23)	0·29(2)	41·27(18)	0·46(11)	—	—	—	—	100·04(36)
	cpx	3	53·12(27)	0·40(3)	2·43(40)	0·04(4)	5·66(19)	0·13(2)	16·64(21)	21·84(18)	0·15(2)	—	—	—	100·41(23)
	plag	4	46·36(95)	—	34·76(84)	—	0·67(11)	—	0·20(10)	17·81(62)	1·08(31)	0·04(2)	—	—	100·91(20)
SAR5	glass	9	49·99(20)	0·68(6)	17·39(14)	0·00(0)	7·11(12)	0·15(2)	5·36(13)	10·05(20)	2·13(13)	0·44(2)	0·07(4)	4·82(21)	100·19(26)
	ol	5	39·93(6)	0·02(1)	0·17(10)	0·02(1)	15·41(27)	0·26(4)	43·87(24)	0·41(8)	—	—	—	—	100·18(36)
	cpx	6	53·04(46)	0·47(13)	2·83(43)	0·06(3)	5·24(44)	0·10(3)	16·23(50)	22·22(47)	0·26(21)	—	—	—	100·47(38)
SAR7	glass	10	49·97(15)	0·68(7)	16·59(12)	0·01(2)	7·08(10)	0·15(2)	6·16(8)	10·64(9)	1·96(6)	0·42(1)	0·05(3)	4·59(27)	100·74(30)
	ol	7	40·06(36)	0·02(1)	0·06(7)	0·00(0)	13·89(20)	0·25(4)	45·63(30)	0·33(3)	—	—	—	—	100·25(28)
	cpx	9	53·05(58)	0·37(19)	2·53(64)	0·11(2)	4·82(52)	0·10(3)	16·70(58)	22·39(19)	0·20(14)	—	—	—	100·24(26)
SAR9	glass	—	48·87(15)	0·67(7)	15·46(6)	0·03(2)	7·01(23)	0·10(2)	6·94(5)	11·44(8)	1·81(10)	0·40(1)	0·09(3)	—	92·83(32)
	ol	6	40·05(23)	0·03(1)	0·15(18)	0·00(0)	13·17(24)	0·25(4)	45·69(32)	0·38(10)	—	—	—	—	99·77(24)
	cpx	4	53·32(24)	0·33(6)	2·26(39)	0·20(3)	4·40(13)	0·11(3)	17·08(20)	22·51(28)	0·16(6)	—	—	—	100·35(24)
SAR11	glass	1	49·75(–)	0·96(–)	17·83(–)	0·04(–)	8·51(–)	0·13(–)	4·09(–)	10·00(–)	2·30(–)	0·43(–)	0·12(–)	—	94·20(–)
	ol	8	39·28(20)	0·02(1)	0·05(3)	0·01(1)	18·37(21)	0·26(1)	41·42(20)	0·32(3)	—	—	—	—	99·83(24)
	cpx	4	51·19(49)	0·51(3)	4·79(31)	0·06(3)	7·30(11)	0·18(4)	14·39(24)	21·20(7)	0·24(5)	—	—	—	99·85(40)
SAR15	glass	7	49·67(24)	0·72(6)	16·94(15)	0·01(1)	8·18(9)	0·16(2)	5·47(17)	10·64(17)	1·97(11)	0·45(1)	0·08(4)	4·15(22)	100·37(33)
	ol	5	39·31(18)	0·02(1)	0·10(9)	0·04(1)	17·83(37)	0·25(3)	42·21(38)	0·38(3)	—	—	—	—	100·16(49)
	cpx	7	52·77(34)	0·38(5)	3·30(59)	0·10(4)	5·64(15)	0·12(2)	16·16(29)	22·57(34)	0·14(6)	—	—	—	101·18(24)
SAR16	glass	6	50·38(31)	0·76(4)	17·09(32)	0·01(1)	8·18(26)	0·15(2)	4·50(34)	9·53(34)	1·95(18)	0·44(3)	0·04(3)	5·10(57)	99·82(20)
	ol	6	38·45(13)	0·03(1)	0·06(2)	0·05(1)	20·73(33)	0·31(2)	39·67(23)	0·34(1)	—	—	—	—	99·69(43)
	cpx	6	52·77(48)	0·36(6)	2·77(52)	0·05(1)	7·06(86)	0·17(2)	16·11(40)	21·54(71)	0·11(2)	—	—	—	100·95(35)
	plag	7	45·48(40)	—	35·15(38)	—	0·78(5)	—	0·15(5)	18·55(18)	0·83(6)	0·03(1)	—	—	100·97(48)
SAR17	glass	1	49·25(–)	0·77(–)	16·61(–)	0·00(–)	8·68(–)	0·14(–)	5·74(–)	10·76(–)	1·62(–)	0·37(–)	0·05(–)	4·53(–)	100·97(–)
	ol	5	39·26(28)	0·01(1)	0·06(2)	0·04(2)	17·41(43)	0·25(2)	42·43(35)	0·35(4)	—	—	—	—	99·85(44)
	cpx	6	51·15(65)	0·54(6)	4·97(63)	0·13(4)	5·96(45)	0·14(4)	15·55(35)	21·74(32)	0·14(2)	—	—	—	100·32(70)

Values are in weight per cent and are averages with standard deviation in parentheses such that 47·85(22) should be read as $47·85 \pm 0·22$. *n*, number of analyses averaged. —, not analyzed.
*H_2O values are based upon calibrating H_2O by summation deficit against SIMS analyses: $H_2O = 0·73(100 - \text{sum})$.

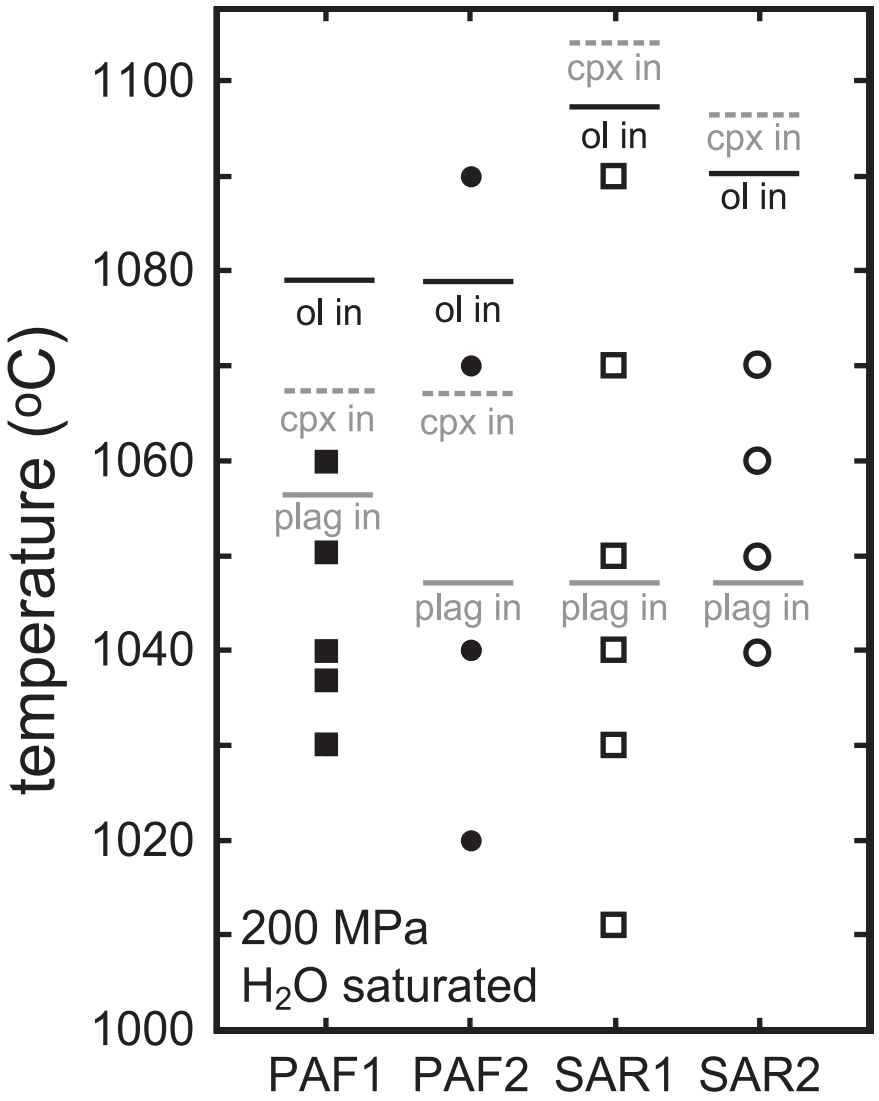

Fig. 2. Crystallization sequences at 2 kbar, H_2O-saturated conditions of the four compositions used in this study (see Tables 1 and 2 for details). The relative position of the ol-in versus the cpx-in boundary was directly determined only for one composition (PAF2). The others were inferred from the slopes of the LLDs (Fig. 3) and from the results of experiments that lost too much FeO to be considered successful (and are not reported in the tables), but should give the correct crystallization sequence.

has on it, that we will exploit to estimate pre-eruptive H_2O concentrations. The more H_2O in the magma, the more plagioclase saturation will be delayed, and the higher the peak in the Al_2O_3 LLD will become. For PAF, the maximum Al_2O_3 concentration reached along the LLD ($Al_2O_3^{max}$) is 18·5 wt %, slightly lower than that reached by the SAR compositions ($Al_2O_3^{max} = 19$ wt %). For most of the paths, there is also little difference between the different versions of the starting compositions (i.e. PAF1 vs PAF2). Thus, as a first approximation, we will attribute all changes in $Al_2O_3^{max}$ to H_2O. As the experiments and whole-rock database improve, effects of changing other bulk composition components (SiO_2, alkalis, etc.) may be considered.

None of the experiments are exactly at the plag-in point, and so $Al_2O_3^{max}$ values need to be estimated. One option is to use the slopes of the LLD before and after the plag-in point to estimate the plag-in point (where the two lines meet). However, this introduces considerable errors and can lead to both high and low estimates. In addition, the temperature and composition of the melt at the plag-in point also need to be estimated in this method. To be conservative, we have simply taken $Al_2O_3^{max}$ as the measured experimental melt with the highest Al_2O_3, without any correction. This means that our $Al_2O_3^{max}$ values are lower bounds on the true $Al_2O_3^{max}$ values.

For comparison with the measured LLDs, fractionation paths for the PAF2 and SAR2 compositions were

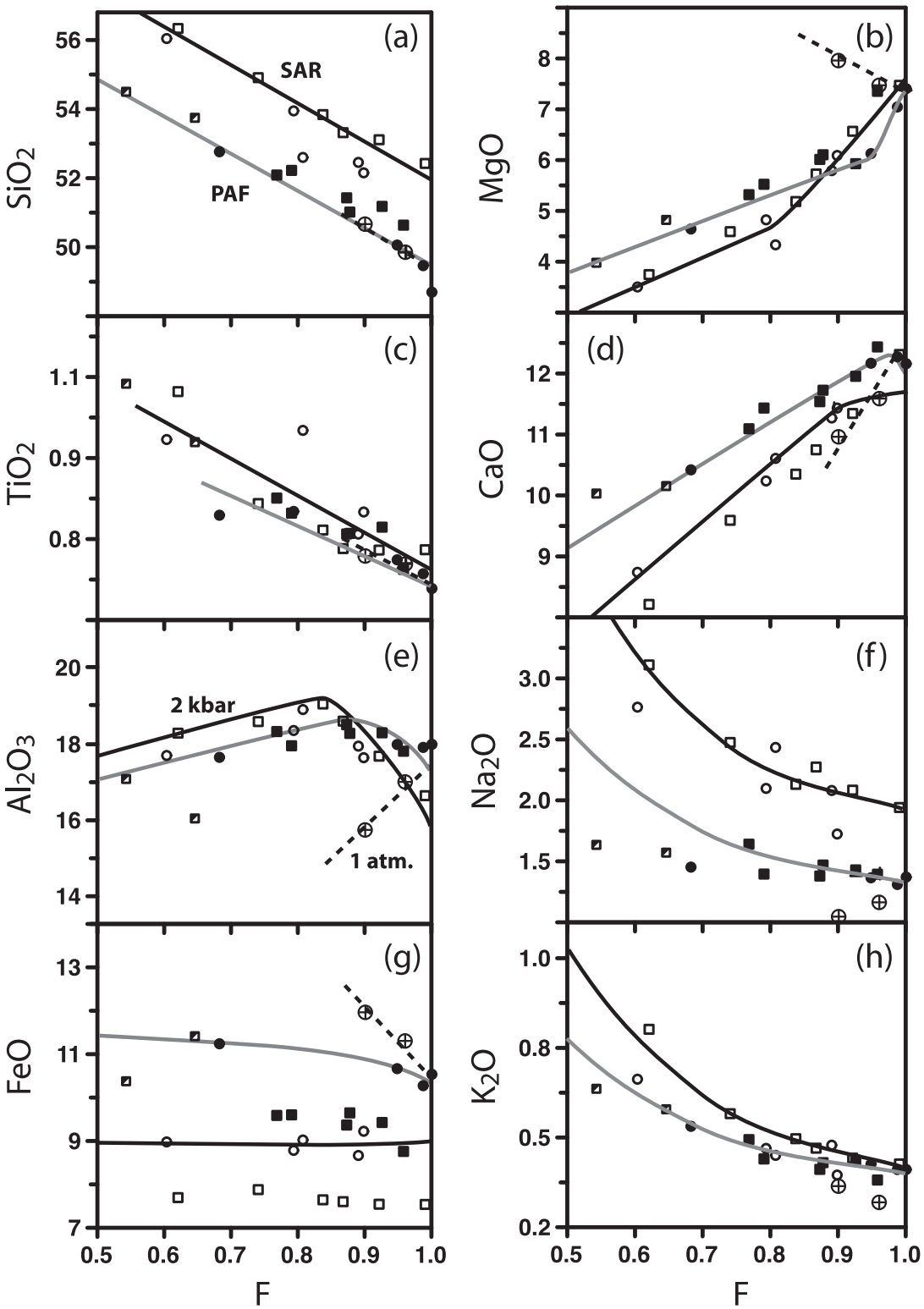

Fig. 3. Melt compositions vs per cent melt (*F*, determined by mass balance) for experiments on compositions PAF1 (filled squares), PAF2 (filled circles), SAR1 (open squares) and SAR2 (open circles). Half-filled squares are 1 kbar experiments on PAF1. Circles with crosses are the two anhydrous experiments using the PAF2 composition. Liquid lines of descent are inferred for Sarigan (black line) and Pagan (gray line) and were drawn by eye. Also shown are calculated anhydrous LLDs at 1 bar using the MELTs program (dashed line; also see online material). The calculated and experimental anhydrous results agree well for most oxides, except for K_2O and Na_2O. These are low in the experiments owing to their volatilization during the runs. The largest difference between the hydrous and anhydrous LLDs are for Al_2O_3, FeO and, to a lesser extent, CaO. Glass compositions are plotted on an anhydrous basis for comparison with the Mariana lavas.

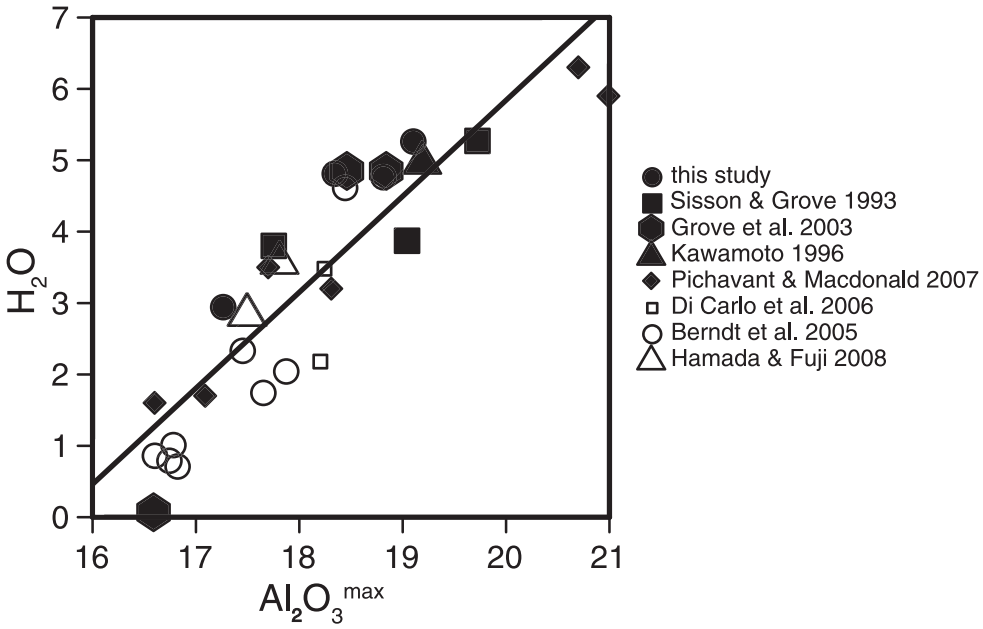

Fig. 4. H_2O (values corrected to ion probe data) vs maximum Al_2O_3 concentrations of the magma before plagioclase saturation. Each point represents a different bulk composition. Experiments were performed over a range of pressures from 1 atm to 5 kbar in gas pressure vessels (internally and externally heated). Linear regression yields the equations $H_2O_{plag\text{-}in} = 1{\cdot}34Al_2O_3^{max} - 21{\cdot}05$. This is the relationship used to calculate $H_2O_{plag\text{-}in}$ for the Mariana arc magmas.

calculated using the MELTs thermodynamic program (Ghiorso & Sack, 1995; Asimow & Ghiorso, 1998). MELTs does a good job of reproducing the anhydrous Al_2O_3 LLDs (online Fig. 2 and Table 3). However, in the hydrous models, plagioclase saturation occurs substantially later than observed in the experiments, resulting in LLDs that rise to significantly higher Al_2O_3 than the observed LLDs.

In this study, we focus exclusively on using Al_2O_3 LLDs to estimate pre-eruptive H_2O. Both FeO and, to a lesser extent, CaO are also potentially useful. However, whereas FeO in the experiments is well behaved, the whole-rock data for FeO are highly scattered, perhaps as a result of magnetite crystallization, and do not provide clear results at this point. For CaO, there is a noticeable separation between the dry and wet LLDs. However, the difference is small in magnitude and the direction of plag crystallization is similar to that of cpx crystallization, making it difficult to disentangle. Thus we focus on Al_2O_3 here.

As expected, the plag-in point correlates with the H_2O content of the melts. The experimentally produced Mariana LLDs show a rise in $Al_2O_3^{max}$ from 17·2 wt % at 2·8 wt % H_2O to 19·1 wt % at 5·2 wt % H_2O. To expand the compositional range of the data for our parameterization, $Al_2O_3^{max}$ values in published studies have been assembled (Fig. 4). The $Al_2O_3^{max}$ values were estimated in the same way as for our experiments, using the experiment with the highest Al_2O_3 melt for a given bulk composition. For the experiments of Pichavant & Macdonald (2007) and di Carlo *et al.* (2006) we use their published H_2O contents, which are based on SIMS calibrated microprobe analyses. For the remaining studies without SIMS data, we use the SIMS calibration for our microprobe ($H_2O = 0{\cdot}73H_2O$ by difference) on the published microprobe analyses of the melts. In the absence of SIMS calibrations of the various microprobes involved, we feel that applying the same equation to all of the literature data at least provides consistency.

Fitting the data (online Table 1) for $Al_2O_3^{max}$ yields the equation $H_2O_{plag\text{-}in} = 1{\cdot}34Al_2O_3^{max} - 21{\cdot}05$. Stepwise linear regression was used to explore whether adding other components would improve the fit. The best results were for a combination of $Al_2O_3^{max}$, Mg, and Na + K. However, the differences between the two fits is small. Both have errors of about ±1 wt % H_2O and so we use the simpler model in this paper.

LLDS IN MARIANA LAVA SUITES

The primary difficulty with using LLDs to estimate pre-eruptive H_2O contents is finding one. That is, it is not obvious that any suite of arc lavas ever records a pure LLD, unaffected by crystal accumulation or magma mixing. All petrographic studies of arc magmas reveal some combination of complexly zoned crystals, multiple phenocryst generations, resorption features, reverse zoning, reaction rims and other evidence for crystal

accumulation and magma mixing. Trace element and isotopic studies also show evidence for magma mixing. We must see through these processes, or at least minimize them, if we are to apply the LLD approach to estimating pre-eruptive H_2O.

We use three criteria to identify LLDs: (1) Eu anomalies relative to the rare earth elements (REE); (2) Sr anomalies relative to the REE; (3) Sr, Nd and Pb isotopic composition. Criteria 1 and 2 are aimed at identifying magmas that have accumulated plagioclase. We assume that olivine and pyroxene are the initial crystallizing phases. Their crystallization will increase the Al_2O_3 concentration of the melt. As described above, the higher the H_2O concentration of the magma, the higher the Al_2O_3 can build up before plagioclase begins to crystallize. However, accumulated plagioclase will also increase the Al_2O_3 concentration of the bulk-rock. If this composition is assumed to be a melt composition (which it is not) and is used in the equations to estimate H_2O concentrations, the estimated H_2O will be artificially high. However, plagioclase is rich in Sr and Eu, and so its accumulation into a magma will generate positive Sr and Eu anomalies relative to the REE. Criteria 1 and 2 allow one to distinguish between an Al_2O_3 increase owing to olivine and pyroxene crystallization and an Al_2O_3 increase owing to plagioclase accumulation. Criterion 3 allows one to identify whether magmas along an apparent LLD in fact have the same parental magma. All of the data used in the following analysis were downloaded from the GeoRoc website (precompiled files for Mariana islands and seamounts, downloaded July 2007, http://georoc.mpch-mainz.gwdg.de/georoc/) and can be found in the online supplementary material (Supplementary Data Tables 4 and 5).

Criterion 1 (Eu)

We assume that prior to plagioclase crystallization, the magma had a smooth REE pattern, with no Eu anomaly. Some primitive New Britain arc lavas have positive Eu anomalies that are not due to plagioclase addition, but this appears to be an exception (Woodhead *et al.*, 1998). We measure the size of the Eu anomaly relative to the REE using the linear-scale equation $Eu/Eu^* = 2Eu/(Sm + Gd)$, where Eu* represents the expected Eu concentration if there were no Eu anomaly. Using the log-scale equation $[Eu/Eu^* = Eu/(Sm \times Gd)^{0.5}]$ does not change the results. Olivine and pyroxene crystallization will not fractionate Eu from the other REE and so will not produce an anomaly. In contrast, plagioclase has a high partition coefficient for Eu (Drake & Weill, 1975; Aigner-Torres *et al.*, 2007) and so once it begins to crystallize it will impart a negative Eu anomaly ($Eu/Eu^* < 1$) in the REE pattern of the magma. Conversely, accumulation of plagioclase (from other melt volumes) will produce positive Eu anomalies ($Eu/Eu^* > 1$; Woodhead, 1988). Thus, all magmas along a true LLD will have $Eu/Eu^* \leq 1$ (assuming they did not start with an Eu/Eu* anomaly). The high D^{Eu} value (relative to the REE) occurs because Eu occurs as both Eu^{3+} and Eu^{2+}. We make no assumptions about the exact Eu^{3+}/Eu^{2+} value, other than that some Eu^{2+} is present to increase the D value.

Of course, this does not guarantee that the melt has not accumulated any plagioclase. For example, if a magma fractionates a given amount of plagioclase (10%, for example) and then has half that amount added back by accumulation (5%), the Eu/Eu* of the magma will still be less than unity, even though it has accumulated plagioclase. The critical point, however, is that its Al_2O_3 will not rise above the $Al_2O_3^{max}$ value that would be produced by fractionation alone (which records the H_2O concentrations). In this case, the estimated H_2O concentrations will be lower than the true H_2O concentration. Therefore, in general, the LLD method will be a conservative estimate of the pre-eruptive H_2O concentration of the magmas.

To assess the effect of the Eu filter on the data, we apply two upper Eu/Eu* limits: one strict (0·98) and one loose (1·02), and observe the effects on the apparent LLDs (Fig. 5). The unfiltered samples from the Mariana islands have maximum Al_2O_3 concentrations of 21–22 wt %. Applying the $Eu/Eu^* < 1{\cdot}02$ to the data removes many, although not all, of the data above 20 wt % Al_2O_3. A number of samples that plot at high Mg-number and high Al_2O_3 (upper right of Fig. 5) were also removed, producing a fairly sharp boundary on the right side of the data in Fig. 5. The filtered data fill a well-defined triangular region with its apex at an Mg-number of 0·4 and Al_2O_3 of 20 wt %. This is what would be expected of an LLD, with the right side of the triangle representing the plagioclase-absent early fractionation of the melt and the left side of the triangle representing the decrease of Al_2O_3 owing to plagioclase fractionation. Samples in the interior of the triangle could either be melts that fractionated plagioclase earlier (owing to lower H_2O concentrations) or could be mixtures between melts on opposite sides of the triangle (fractionated with unfractionated). Applying the $Eu/Eu^* < 0{\cdot}98$ filter removes all of the samples with $Al_2O_3 > 20$ wt %, and sharpens the right side boundary of the data, but does not significantly change the shape of the dataset.

The unfiltered dataset from seamounts displays much clearer LLDs than the island data, with an already clearly distinguished triangular shape. As with the island data, the $Eu/Eu^* < 1{\cdot}02$ filter removes most of the data with $Al_2O_3 > 20$ wt %, and the $Eu/Eu^* < 0{\cdot}98$ removes the remaining data above 20% Al_2O_3. The data also define a triangular region with the same apex as the island data at Mg-number = 0·4 and $Al_2O_3 = 20$ wt %. What is different from the island data is that the $Eu/Eu^* < 0{\cdot}98$ filter also removes a number of seamount samples at high Mg-number and low Al_2O_3, which appear to be the parental melts to

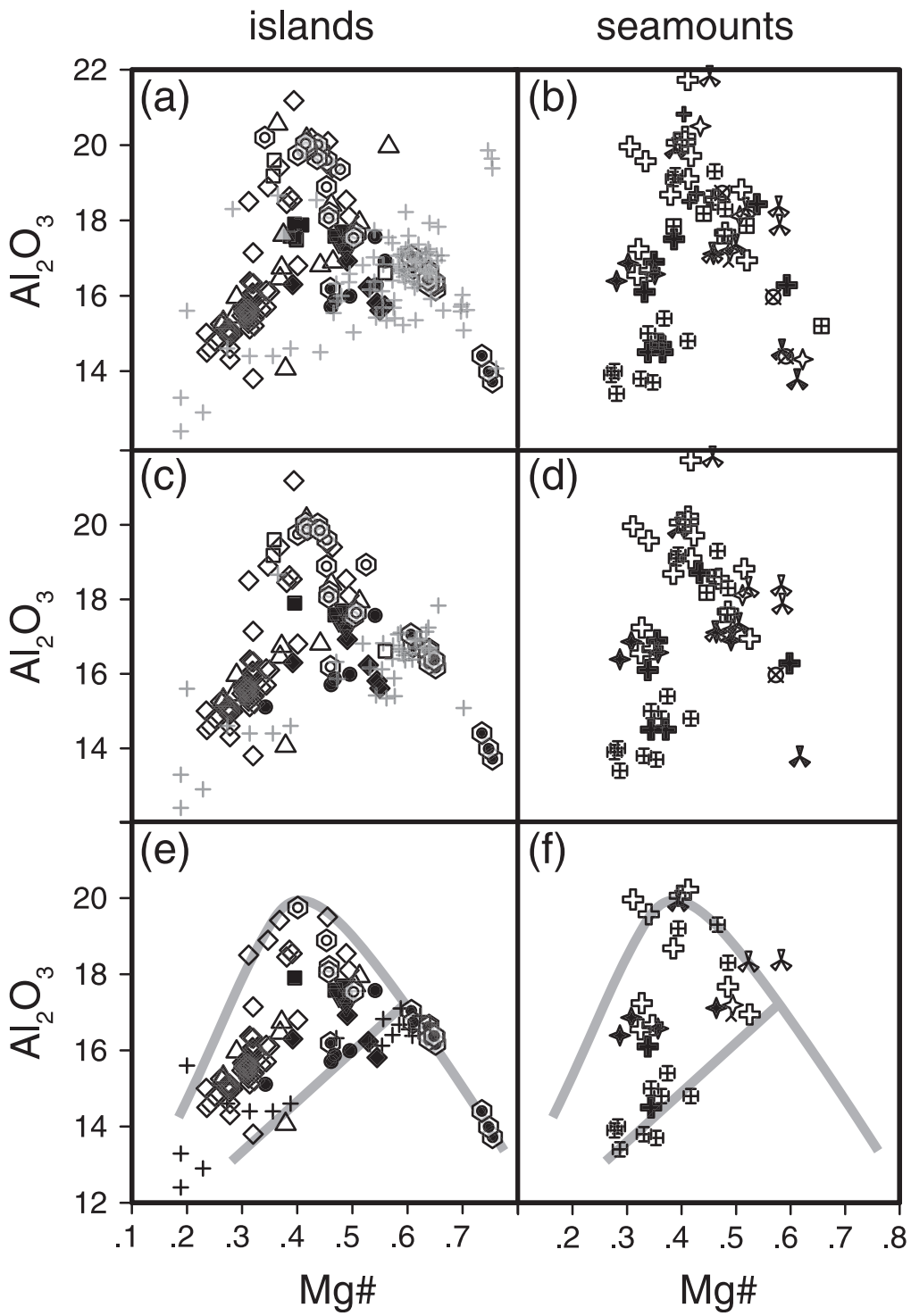

Fig. 5. Compositions of Mariana arc lavas (from GEOROC database, precompiled Mariana arc and Mariana arc seamount files, http://georoc.mpch-mainz.gwdg.de/georoc/, downloaded July 2007). Symbols are same as in Fig. 1. Crosses are Mariana Trough lavas for comparison (also from GEOROC compiled file). (a) Island samples with TE analysis but not filtered. (b) Seamount samples with TE analyses but not filtered. (c) Island samples with Eu/Eu* < 1·02. (d) Seamount samples with Eu/Eu* < 1·02. (e) Island samples with Eu/Eu* < 0·98. (f) Seamount samples with Eu/Eu* < 0·98. The improvement in the definition (sharper peak, clearly defined left and right sides of triangular region) of the LLD in the islands produced by the Eu filter should be noted. Both the island and seamount data have similar apexes at ~20 wt % Al_2O_3 and ~0·4 Mg-number. In (e) and (f) the gray lines show high (6 wt %) and low (2–3 wt %) H_2O LLDs.

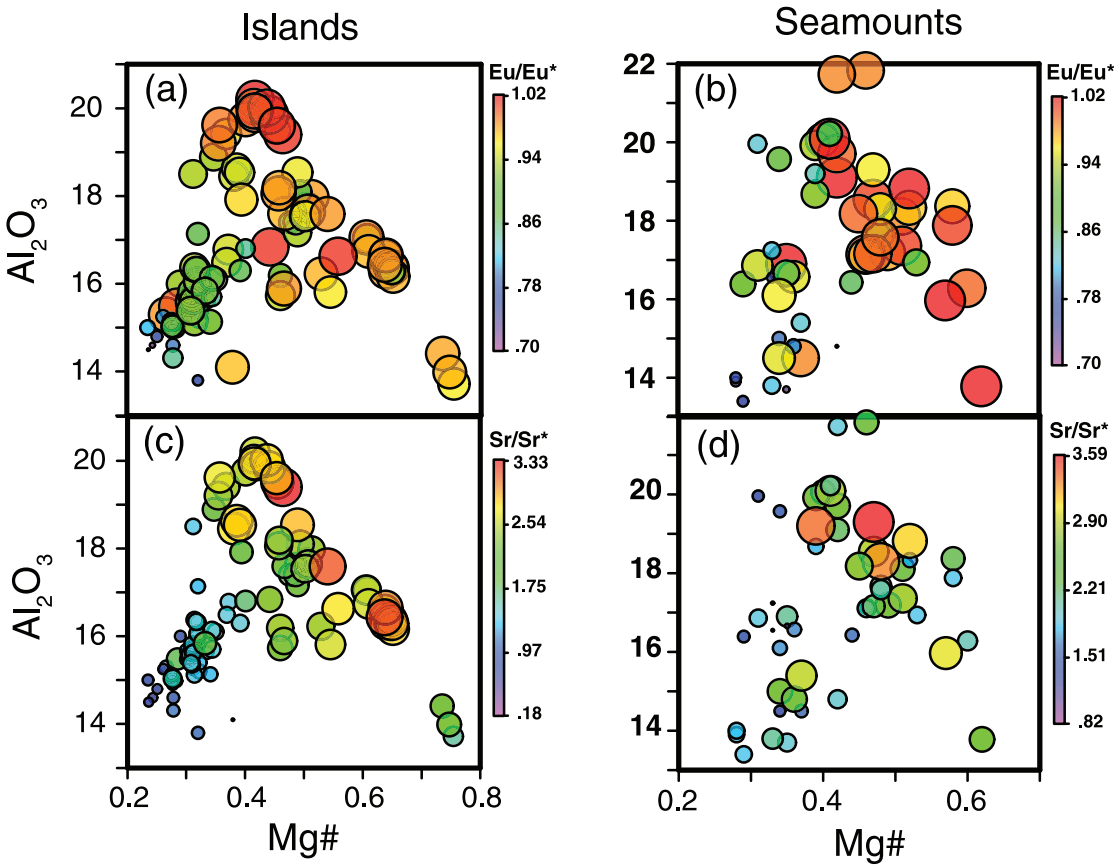

Fig. 6. Variation of Eu and Sr anomalies along the Al_2O_3 LLD (Al_2O_3 vs Mg-number). The size and color of the symbols is proportional to the size of the Eu (a, b) and Sr (c, d) anomalies. Colorscale is given along the right side of each plot. (a, c) Islands; (b, d) seamounts. Along the right side of the triangular-shaped data field (in both islands and seamounts) the Eu and Sr anomalies are constant, consistent with this being the plagioclase-absent limb of the LLD. If the Al_2O_3 increase was due to plagioclase accumulation, there would be a significant rise in Eu/Eu* and Sr/Sr* (larger symbols) with increasing Al_2O_3 contents, but this is not seen. Once plagioclase begins to crystallize (lowering Al_2O_3 as Mg-number decreases), the Eu and Sr anomalies decrease, again suggesting that the data are close to an LLD.

the rest of the magmas. Thus the Eu/Eu* < 0·98 appears to be useful for finding the maximum Al_2O_3 concentration, but in general is too restrictive as parental magmas with no Eu anomaly (Eu/Eu* = 1) are removed.

Criterion 2

This is not used as a filter to remove data, but to check that the Eu filter is working. It is similar to criterion 1 in that plagioclase also has a high partition coefficient for Sr (Drake & Weill, 1975; Aigner-Torres *et al.*, 2007). However, unlike Eu, we cannot assume that there was no Sr/REE anomaly prior to crystal fractionation; so instead, the criterion is simply that the Sr/Sr* value should not rise along the LLD. If it does, it implies that the rise in Al_2O_3 is caused by plagioclase accumulation rather than olivine + pyroxene crystallization. For the Eu* = 1·02 filtered island and seamount data, Sr/Sr* [=2Sr/(Sm + Nd)] shows no rise along the ol + px portion of the LLD (Fig. 6). As with Eu/Eu*, Sr/Sr* decreases strongly after the maximum Al_2O_3 concentration is reached, consistent with plagioclase fractionation.

Criterion 3

This is aimed at assessing the extent of magma mixing. Strictly defined, magmas along an LLD should have a single parental magma with a single isotopic composition. As heavy isotopes are not fractionated by crystallization, all of the magmas in an LLD should have the same isotopic composition and there should be no correlation between the major elements and isotopic ratios. If there are large isotopic changes along an apparent LLD, then the variation in the data may be dominated by mixing of two melts (with different Al_2O_3 and Mg-numbers), rather than fractionation processes. All of the island and seamount data have similar isotopic compositions (Fig. 7). Interestingly, whereas samples from Guguan and the cross-chain seamounts to the west (West Guguan, Guguan 2; Stern *et al.*, 2006) fall on the same Al_2O_3 LLD, they

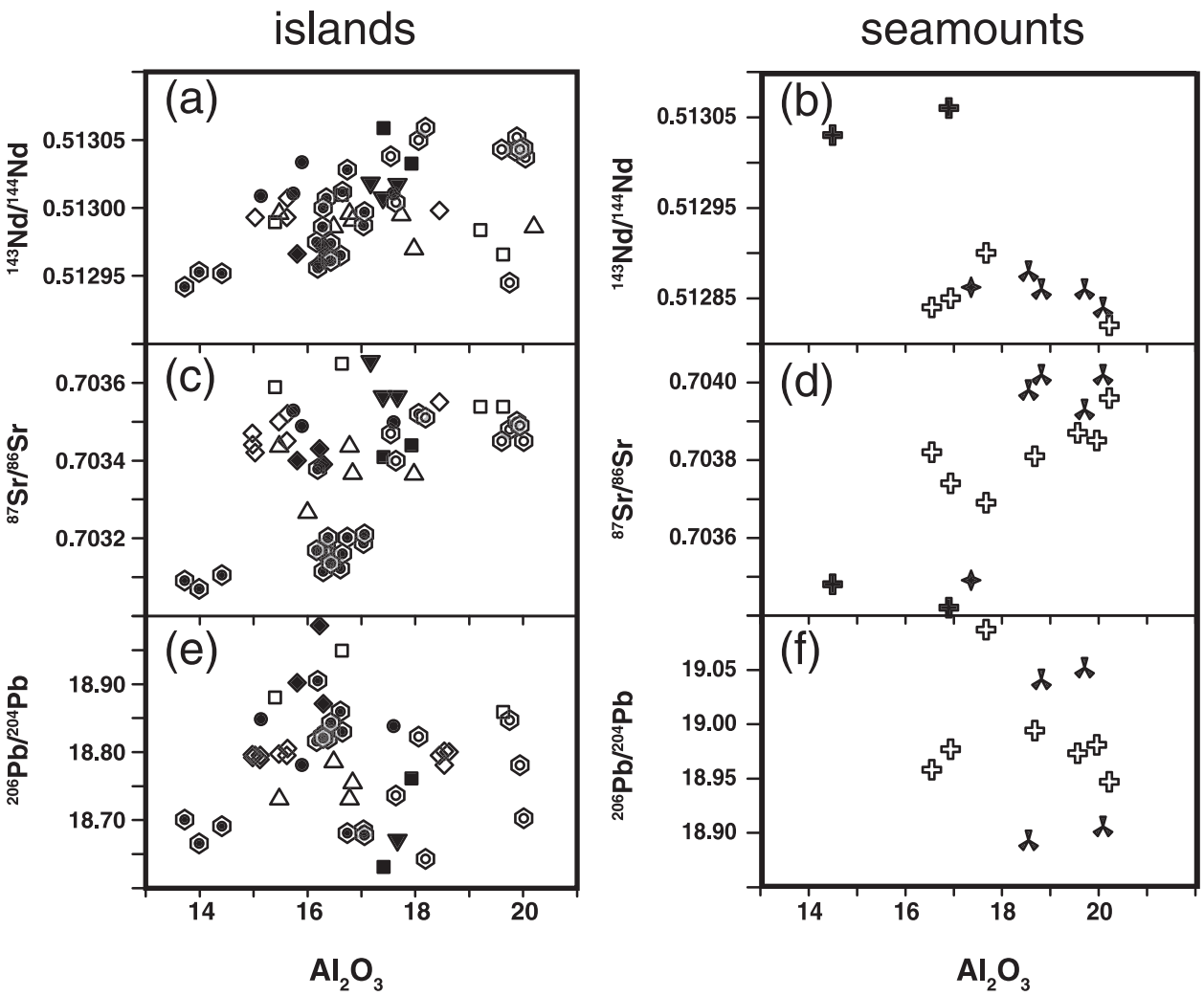

Fig. 7. Nd (a, b), Sr (c, d) and Pb (e, f) isotopic composition of Mariana island (a, c, e) and seamount (b, d, f) samples vs Al_2O_3. Magmas along an LLD should have the same isotopic composition. This is what is observed in the Eu/Eu* < 1·02 filtered data. Guguan island data (open circle within hexagon) are isotopically distinct from the Guguan cross-chain seamounts (filled circle within hexagon). Symbols as in Fig. 1.

have very different Sr and Nd isotopic compositions (although strangely not Pb). The cross-chain volcanoes have lower $^{143}Nd/^{144}Nd$ and $^{87}Sr/^{86}Sr$ ratios. This is also odd because in general Nd and Sr isotopes should be anti-correlated. In any case, there is no correlation between Al_2O_3 and isotopic composition in the magmas, consistent with the compositional trends being near LLDs.

Overall, the Eu/Eu* filter appears to be fairly effective in removing the major effects of plagioclase accumulation, as indicated by Sr/Sr* and Sr, Nd and Pb isotopes. That is not to say that all (or any) of the filtered data are pristine magmas. They probably have all been affected by crystal accumulation and magma mixing to some extent, but not enough to shift them away from the original LLD. The main drawback to the Eu filter is that it requires samples to be analyzed for REE and Sr (as well as major elements). This is true for 44% of the Mariana samples (248 out of 568) with major element analyses. In some cases, there are few (Uracas) or no (Maug) samples that pass the Eu/Eu* filter. In other cases (Sarigan), although some samples pass the filter, there are a number of higher Al_2O_3 samples that do not have REE data. These appear to plot along the LLD defined by the other Mariana magmas, but the REE data are needed to make sure there has not been significant plagioclase accumulation.

Looking more closely at the data, the Mariana lavas appear to be divided into two general groups (Fig. 5). The LLDs of one group rises to an $Al_2O_3^{max}$ of 19–20 wt % Al_2O_3 at an Mg-number of 0·40–0·43. Islands and seamounts that follow this LLD are Guguan, Uracas, Agrigan, Anatahan, Daikoku, Eifuku, USM3 and Hiyoshi. In contrast, the Al_2O_3 concentration of the

Table 4: Estimates of pre-eruptive H_2O contents of arc-related magmas

Arc	Volcano	Lat. (°N)	Al_2O_3 max.[1]	H_2O LLD	H_2O MI	Al_2O_3 MI	H_2O MI frac. corr.	Ref. for MI
Mariana	Agrigan	18·8	20·2	6·1	5·1	16·9	6·5	Kelley *et al.*, 2010
Mariana	Guguan	17·3	20	5·9	4·5	16·3	5·5	Kelley *et al.*, 2010
Mariana	Pagan	18·1	17·6	2·6	3·5	15·5	3·9	Kelley *et al.*, 2010
Mariana	Anatahan	16·4	19·5	5·2	3·4	15·3	4·3	Shaw *et al.*, 2008
Mariana	Asuncion	19·7	17·9	3	4·3	18·5	4·2	Shaw *et al.*, 2008
Mariana	Sarigan	16·7	16·9	1·7	6·1	16	6·5	Kelley *et al.*, 2010
Mariana	Sarigan	16·7	19·6	5·4	6·1	16	7·5	Kelley *et al.*, 2010
Mariana	Uracas	20·5	19·6	5·3	—	—	—	—
Mariana	Alamagan	17·6	17·7	2·7	4·7	17·6	4·7	Shaw *et al.*, 2008
Mariana	Ahyi	20·4	18·1	3·3	—	—	—	—
Mariana	Central Hiyoshi	23·3	20·1	5·9	—	—	—	—
Mariana	Cheref	19·4	19·1	4·6	—	—	—	—
Mariana	Eifuku	21·4	19·9	5·7	—	—	—	—
Mariana	Esmeralda	15	16·9	1·7	—	—	—	—
Mariana	Fukujin	21·9	18·7	4·1	3·3	13·5	4·6	Newman *et al.*, 2000
Mariana	South Daikoku	21	18·8	4·3	—	—	—	—
Mariana	South Hiyoshi	23·2	20·2	6·1	—	—	—	—
Mariana	USM3	22	19·3	4·9	—	—	—	—
Mariana	Diamante	15·9	18·2	3·4	—	—	—	—
Mariana	trough	12–22	17·8	2·9	2·2	17·9	2·2	Newman *et al.*, 2000
Cental America	Arenal	10·5	20·7	6·8	3·9	18	4·5	Wade *et al.*, 2006
Cental America	Pacaya	14·4	20·2	6·1	2·4	—	—	Walker *et al.*, 2003
Cental America	Irazu	10	17·7	2·8	3·3	19·2	3	Benjamin *et al.*, 2007
Cascades	Medicine Lake	41·6	17·3	2·2	2·1	15·8	2·3	Anderson, 1973
Italy	Stromboli	38·8	18·7	4·1	3·5	14·4	4·6	Bertagnini *et al.*, 2003
Andaman	Barren Island	12·3	18·7	4·1	3·4	16·9	3·7	Luhr & Haldar, 2006
Not Eu filtered*								
Central America	Cerro Negro	12·5	20·6	6·7	6	18·3	6·8	Roggensack *et al.*, 2001
Central America	Fuego	14·5	19·7	5·4	6	16·6	5·7	Roggensack *et al.*, 2001
Cascades	Shasta	41·4	19	4·5	3·7	16	4·39	Anderson, 1973

[1]Bulk-rock data from GeoRoc (see text).
MI data from Anderson (1973), Newman *et al.* (2000), Roggensack (2001), Bertagnini *et al.* (2003), Walker *et al.* (2003), Luhr & Haldar (2006), Wade *et al.* (2006), Benjamin *et al.* (2007), Shaw *et al.* (2008) and Kelley *et al.* (2010).

second group has a lower Al_2O_{3max} of ~17 wt % at an Mg-number of 0·55–0·6. This group includes Pagan, Alamagan, Sarigan, Asuncion, and Daikoku. Although our analysis is focused on the Mariana arc, it is interesting to note that this low Al_2O_3 group falls along the trend defined by Mariana trough (back-arc) magmas (Fig. 5).

COMPARISON WITH MELT-INCLUSION ANALYSES

Pre-eruptive H_2O concentrations for the Mariana magmas are calculated using the linear model from Fig. 4 and the LLDs from Fig. 5 (Table 4). For each island and seamount, the sample (filtered as described above) with the highest Al_2O_3 ($Al_2O_3^{max}$) is used in the calculation. Therefore the estimates here are for the maximum H_2O concentrations ($H_2O_{plag\text{-}in}$) that are recorded in the LLDs at the plag-in point. Potentially the islands and seamounts could have magmas with variable H_2O concentrations. These LLDs would fill the interior of the triangular region in Fig. 5. The problem is that these would be difficult to distinguish from magmas that had simply mixed with a much more evolved magma. Thus although localities such as Anatahan and USM3 show some evidence of variable

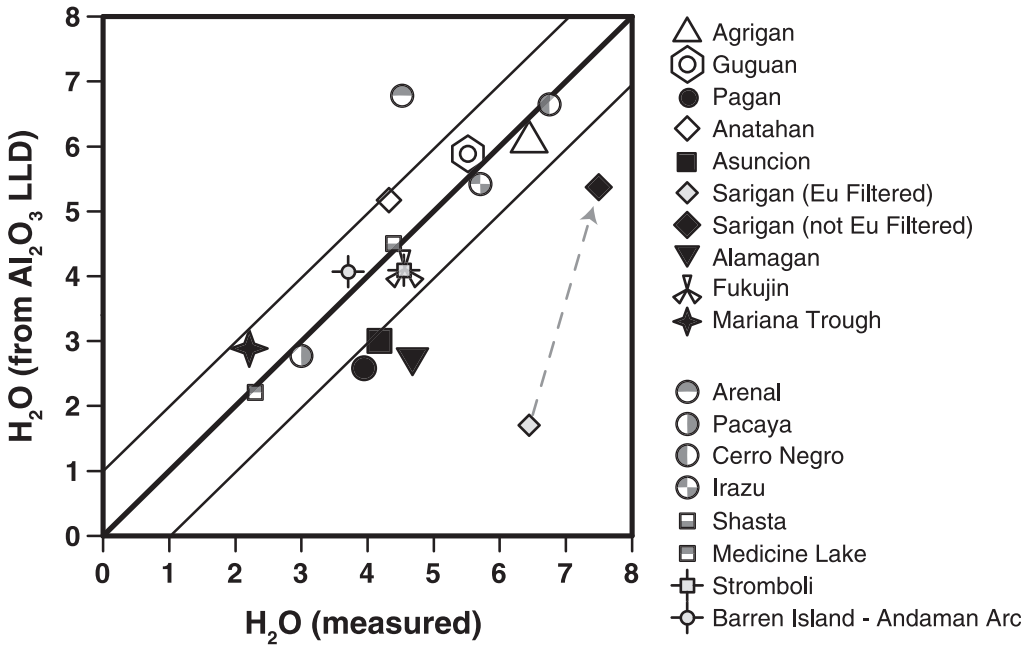

Fig. 8. $H_2O_{plag\text{-}in}$ estimated from the observed Al_2O_3 LLD vs the maximum H_2O measured in glassy, olivine-hosted melt inclusions (Table 4). The MI H_2O analyses have been fractionated to the Al_2O_{3max} value (see text). Mariana symbols as in Fig. 1. The LLD estimate of H_2O_{max} for Sarigan (1·6 wt %, gray filled diamond) is much lower than observed in melt inclusions (6·1 wt %). However, this is probably due to the lack of TE data for many Sarigan samples. There are Sarigan samples with LLD H_2O_{max} of >5 wt %, but they do not have TE analyses. If these unfiltered Sarigan data are used (black filled diamond), all data fall within 2 wt % of the 1:1 line. Most data are within 1 wt %.

H_2O concentrations in their LLDs, this is impossible to confirm with the present analysis and so we focus on the maximum H_2O recorded by the magmas ($H_2O_{plag\text{-}in}$). It should be noted that the H_2O_{max} value is the value for the plag-in point. If the magma is not vapor-saturated at this point, H_2O concentrations will continue to rise as fractionation proceeds. The calculations produce estimates of $H_2O_{plag\text{-}in}$ between 1·5 and 6 wt % for Mariana magmas (Figs 8 and 9).

To test the LLD estimates, we compare the LLD estimates of $H_2O_{plag\text{-}in}$ with the H_2O measured in olivine-hosted melt inclusions (Table 4). Glassy, olivine-hosted melt inclusions (MI) from seven Mariana islands (Guguan, Agrigan, Anatahan, Alamagan, Asuncion, Pagan and Sarigan) and one seamount (Fukujin) have been analyzed for volatile and major element concentrations (Newman *et al.*, 2000; Shaw *et al.*, 2008; Kelley *et al.*, 2010). Assuming no post-entrapment volatile loss or gain, the melt inclusions record the H_2O content of the melt at the time of the olivine growth. This is unlikely to be at the plagioclase-in boundary and so the measured H_2O contents in the MI will not be equivalent to the LLD-based estimates (which predict the H_2O content at the plag-in boundary). To make the comparison, the MIs are fractionated until their Al_2O_3 contents match the $Al_2O_3{}^{max}$ value found in the bulk-rock LLD. To keep the corrections as simple as possible, we assume a constant H_2O/Al_2O_3 ratio (taken from the melt inclusion) and use that to calculate the H_2O at the plag-in boundary using the Al_2O_{3max} from the bulk-rock LLDs. Because H_2O and Al_2O_3 are highly incompatible in olivine and clinopyroxene, the H_2O/Al_2O_3 ratio will not change substantially between the entrapment of the melt inclusion and the plag-in boundary. The magnitude of the corrections range from 0 to 1·4 wt % H_2O (Table 4). With the notable exception of Sarigan, all of the samples fall within 2 wt % of the 1:1 line (Fig. 8). Given the inherent uncertainties in locating the plag-in boundary in both the experimental and natural LLDs, a 1–2 wt % error seems reasonable. Sarigan is far from the 1:1 line and merits more discussion.

The Sarigan LLD reaches a maximum Al_2O_3 just above 17 wt % (Fig. 5), which implies H_2O concentrations of 2–3 wt %. However, the Sarigan MIs contain up to 6% H_2O. Given that the major element compositions of the Sarigan magmas are similar to those of other Mariana magmas, and that it was one of the compositions used to calibrate the model, it seems unlikely that the error is in the experimentally calibrated hygrometer equation. Looking at all of the Sarigan whole-rock data (both with and without REE data), there are a number of samples with high Al_2O_3 that plot along the LLD defined by other Mariana lavas. However, because these samples have not been analyzed for TE, they cannot be assessed for plagioclase fractionation at this point (and so were not

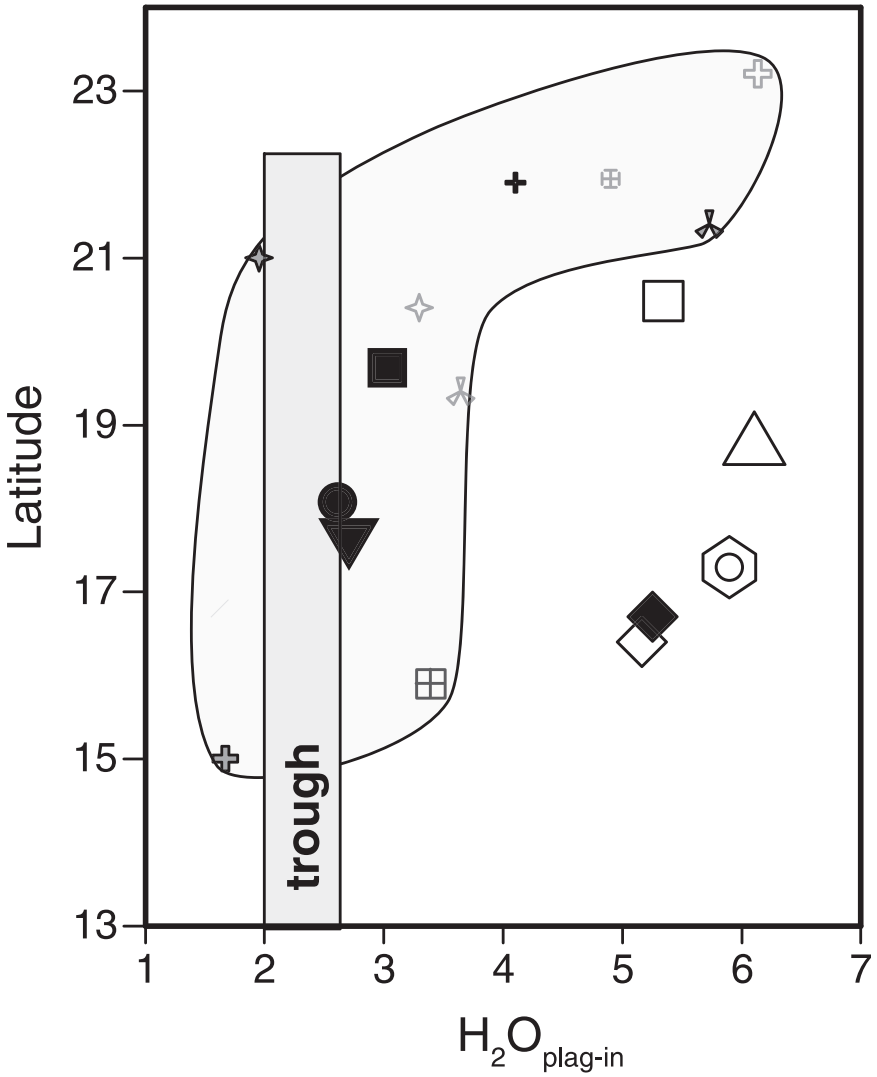

Fig. 9. Variation of $H_2O_{plag\text{-}in}$ in Marina arc islands and seamounts vs latitude. Grey bar indicates $H_2O_{plag\text{-}in}$ for Mariana Trough magmas (Newman *et al.*, 2000). There is no systematic along-arc variation in $H_2O_{plag\text{-}in}$. The lowest $H_2O_{plag\text{-}in}$ in the arc are similar to the $H_2O_{plag\text{-}in}$ of the Mariana back-arc. The highest $H_2O_{plag\text{-}in}$ for islands and seamounts are ~6 wt %.

included in the figures). If we assume that at least some of the high Al_2O_3 Sarigan samples have not accumulated plagioclase, then their H_2O_{max} estimate from the LLD would be 5·4 wt %, consistent with the values measured in the MIs from Sarigan (Fig. 8). At this point, this is our preferred explanation, although clearly the TE composition of the high Al_2O_3 Sarigan samples need to be analyzed to confirm this.

The Sarigan case illustrates one of the main uncertainties involved in using the LLD method. The method requires extensive sampling and geochemical analysis of each island or volcano. The fewer the samples, the more likely it is that the peak Al_2O_3 samples will be missed. This will produce underestimates of $Al_2O_3{}^{max}$ and $H_2O_{plag\text{-}in}$. In Fig. 8, this will result in points being shifted to the right of the 1:1 line (assuming the MI data are correct). Indeed, the three samples that fall farthest to the right of the 1:1 line are islands with the fewest samples that pass the geochemical tests described above: Sarigan (four samples), Alamagan three) and Asuncion (three). Thus one prediction is that with more sampling and analyses, higher Al_2O_3 non-cumulate samples will be found on these islands.

This sampling limitation is also true of the MI data. The fewer the samples, the more likely it is that the highest H_2O samples are missed. For example, Kelley *et al.* (2010) reported two MI analyses from Sarigan, with a maximum H_2O of 6·14 wt %, whereas Shaw *et al.* (2008) reported six MI analyses from Sarigan with a maximum H_2O of 3·84 wt %. Undersampling of MIs (producing low MI H_2O concentrations) will shift the points to the left of the 1:1 line in Fig. 8.

To examine the general applicability of the method, LLDs and MIs from a global database were examined (Table 4; Anderson, 1973; Roggensack, 2001; Bertagnini *et al.*, 2003; Walker *et al.*, 2003; Luhr & Haldar, 2006; Wade *et al.*, 2006; Benjamin *et al.*, 2007). Eight volcanoes have enough data to compare: Arenal, Irazu, Cerro Negro, Fuego, Mt. Shasta, Medicine Lake, Stromboli, and Barren Island (Fig. 8). In some cases (Cerro Negro, Fuego and Mt. Shasta), there were too few whole-rock data to use the Eu and Sr filters, and these should be treated with caution (Table 4). Encouragingly, seven of the eight volcanoes plot within 1 wt % H_2O of the 1:1 line. The one exception is Arenal, where the LLD estimated H_2O is 6·6 wt % whereas the MIs (corrected for fractionation) have 4·5 wt % H_2O. Arenal MIs have high CO_2 contents (up to 300 ppm), indicating that they are relatively undegassed with respect to H_2O (Wade *et al.*, 2006). However, the LLD estimates suggest that the MIs have degassed somewhat, and that Arenal has similar H_2O_{max} concentrations to Cerro Negro (6–7 wt %). Some support for this comes from the observation that Arenal and Cerro Negro MIs fall on a consistent H_2O–CO_2 trend (Wade *et al.*, 2006).

In sum, the LLD method is consistent with existing MI data and appears to be a promising alternative for cases where glassy MIs cannot be found. Its main advantage is that it can be applied to nearly any well-sampled volcano and does not require 'special' samples. The downside is that it requires extensive sampling and geochemical analyses to be used properly. Given ideal sampling and analyses, errors on the LLD estimates of $H_2O_{plag\text{-}in}$ are ~1–2 wt % H_2O. Thus it is a semi-quantitative tool at best. More experiments will improve this somewhat, particularly in expanding the method to more alkali-rich samples. The main source of uncertainty comes from identifying LLDs. Indeed, given the ubiquity of crystal accumulation and magma mixing, it is unclear that true LLDs are ever found in nature. Nevertheless, it appears that these processes do not entirely obscure the chemical trends imparted by crystal fractionation (Fig. 5). Careful use of trace elements and isotopes to filter out the most heavily affected samples allows useful information about the initial volatile contents to be extracted from suites of related arc lavas.

ALONG-ARC H_2O_{MAX} VARIATION

With the above caveats in mind, we apply the LLD method to a key question in the study of the Marianas lavas and arc volcanism in general: How do the H_2O concentrations of magmas vary along the arc? Are they uniform, suggesting a fairly constant volatile flux from the slab? Or do the H_2O concentrations vary in relation to some subduction parameter such as slab dip, slab age or subduction obliquity, suggesting regular changes in the amount of volatiles released from the subduction slab?

Our method estimates the H_2O of the melt at plagioclase saturation. To determine the initial H_2O concentration in the melt (prior to any fractionation) requires an estimate of the amount of olivine and pyroxene fractionation. This is beyond the scope of this paper. We assume that the variations in olivine + pyroxene fractionation prior to plag-in are small enough that the H_2O contents at plag-in reflect the variations in the pre-fractionation H_2O contents, although not the absolute values. In general, the olivine-hosted melt inclusions are trapped prior to plag-in, and so their H_2O contents should be lower than the LLD estimates.

Overall, there does not appear to be a strong along-arc trend in $H_2O_{plag\text{-}in}$ in the Marianas (Fig. 9). In the seamounts, H_2O_{max} is between 1·7 and 3·5 wt % along most of the length of the arc. This is similar to the amounts of H_2O seen in Mariana trough magmas (Newman *et al.*, 2000). At ~21°N, the H_2O_{max} of the seamounts appears to increase to a maximum of 6 wt % for the Hiyoshi seamounts. This corresponds to an abrupt change in the isotopic composition of the magmas and has been linked to the subduction of the Wake and Magellan seamounts (Benjamin *et al.*, 2007), and so it is not clear to what extent they can be compared with the main body of the Mariana arc. Thus we exclude the seamounts above 21°N.

Looking at the Mariana islands, three (Asuncion, Pagan, Alamagan) have $H_2O_{plag\text{-}in}$ that is within the range of the seamounts (1·7–3·1 wt %). However, four islands (Uracas, Agrigan, Guguan, Anatahan) have much higher $H_2O_{plag\text{-}in}$ (5·1–6·1 wt %). Unlike the seamounts, these high H_2O_{max} islands are not all in the north, but are distributed more or less randomly along the length of the arc. Sarigan is excluded because of the uncertainty in its H_2O concentrations, but whether it has high or low H_2O will not change the results. The overall impression is of generally homogeneous volatile concentrations in the magmas (seamounts, trough and low H_2O islands) within which are a few localized areas of high volatile concentrations. There appears to be no relation of the high volatile content areas to the changes in slab dip or subduction obliquity that occur along the Mariana arc. Overall, the pattern seen in the Marianas is strikingly similar to that seen in the Central American arc (Walker *et al.*, 2003).

A number of processes could produce the small-scale volatile heterogeneity observed in the islands. First, the flux of H_2O from the slab could be heterogeneous, perhaps related to slab tears or similar localized features (Miller *et al.*, 2006). Second, the flux could be homogeneous, but could become channelized in the sub-arc mantle, perhaps through reactive flow type processes (Kelemen *et al.*, 1997; Spiegelman *et al.*, 2001). Or third, the variations could be due to local differences in the depth of fractionation. The solubility of H_2O in magmas decreases with decreasing pressure. Therefore magmas that pond and fractionate

at greater depths will retain higher H_2O contents than magmas that pond and degas at shallower levels, even if they originally started with the same H_2O contents. In this case, the $H_2O_{plag\text{-}in}$ estimates would not constrain the flux of H_2O from the subducting crust and lithosphere, but would record local fractionation processes. The current data do not distinguish between these various possibilities.

CONCLUSIONS

(1) Al_2O_3 versus Mg-number liquid lines of descent indicate that Mariana arc lavas contain between 2 and 6 wt % H_2O prior to eruption (Fig. 9). There is no evidence in the LLDs or melt inclusions for pre-eruptive H_2O concentrations substantially higher than 6 wt %. Most seamounts and about half of the islands have $H_2O_{plag\text{-}in}$ of 2–3 wt %, very similar to the Mariana Trough. The variations are very similar to what is seen in the Central American arc (Walker *et al.*, 2003).

(2) There does not appear to be any systematic along-arc variation in $H_2O_{plag\text{-}in}$ that can be correlated with a subduction parameter such as slab dip or subduction obliquity (Fig. 9). $H_2O_{plag\text{-}in}$ in the Mariana arc seamounts does increase in the very north of the arc as subduction becomes increasingly oblique and the back-arc approaches the arc and eventually disappears, but isotopic data suggest that this is at least partly related to the subduction of the Wake and Magellan seamounts.

(3) $H_2O_{plag\text{-}in}$ estimated by the Al_2O_3 LLD method corresponds to the maximum H_2O measured in undegassed, glassy melt inclusions (Fig. 8). The correspondence suggests that the Eu and Sr anomaly filters are effective in removing samples with significant amounts of plagioclase accumulation, and that the effects of magma mixing do not entirely obscure the fraction trends of arc lavas.

ACKNOWLEDGEMENTS

Thanks go to Neel Chatterjee for help with the electron microprobe analyses at MIT and to Nobu Shimizu for help with SIMS analyses at WHOI. Reviews by Jon Blundy, Bernie Wood and John Adam, as well as discussions with Colin MacPherson, Jon Davidson and Alberto Saal greatly improved the manuscript.

FUNDING

This research was funded by National Science Foundation grant OCE-0001897.

SUPPLEMENTARY DATA

Supplementary data for this paper are available at *Journal of Petrology* online.

REFERENCES

Aigner-Torres, M., Blundy, J., Ulmer, P. & Pettke, T. (2007). Laser ablation ICPMS study of trace element partitioning between plagioclase and basaltic melts: an experimental approach. *Contributions to Mineralogy and Petrology* **153**, 647–667.

Anderson, A. T. (1973). The before-eruption water content of some high-alumina magmas. *Bulletin of Volcanology* **37**, 530–552.

Asimow, P. D. & Ghiorso, M. S. (1998). Algorithmic modifications extending MELTS to calculate subsolidus phase relations. *American Mineralogist* **83**, 1127–1132.

Baker, D. R. & Eggler, D. H. (1987). Compositions of anhydrous and hydrous melts coexisting with plagioclase, augite, and olivine or low-Ca pyroxene from 1 atm to 8 kbar—application to the Aleutian volcanic center of Atka. *American Mineralogist* **72**, 12–28.

Baker, M. B., Grove, T. L. & Price, R. (1994). Primitive basalts and andesites from the Mt Shasta region, N California—products of varying melt fraction and water-content. *Contributions to Mineralogy and Petrology* **118**, 111–129.

Benjamin, E. R., Plank, T., Wade, J. A., Kelley, K. A., Haun, E. H. & Alvarado, G. E. (2007). High water contents in basaltic magmas from Irazu Volcano, Costa Rica. *Journal of Volcanology and Geothermal Research* **168**, 68–92.

Berndt, J., Koepke, J. & Holtz, F. (2005). An experimental investigation of the influence of water and oxygen fugacity on differentiation of MORB at 200 MPa. *Journal of Petrology* **46**, 135–167.

Bertagnini, A., Metrich, N., Landi, P. & Rosi, M. (2003). Stromboli volcano (Aeolian Archipelago, Italy): An open window on the deep-feeding system of a steady state basaltic volcano. *Journal of Geophysical Research—Solid Earth* **108**, doi:10.1029/2002jb002146.

Bloomer, S. H., Stern, R. J., Fisk, E. & Geschwind, C. H. (1989). Shoshonitic volcanism in the Northern Mariana Arc. 1. Mineralogic and major and trace-element characteristics. *Journal of Geophysical Research—Solid Earth and Planets* **94**, 4469–4496.

Danyushevsky, L. V., McNeill, A. W. & Sobolev, A. V. (2002). Experimental and petrological studies of melt inclusions in phenocrysts from mantle-derived magmas: an overview of techniques, advantages and complications. *Chemical Geology* **183**, 5–24.

Di Carlo, I., Pichavant, M., Rotolo, S. G. & Scaillet, B. (2006). Experimental crystallization of a high-K arc basalt: The golden pumice, Stromboli volcano (Italy). *Journal of Petrology* **47**, 1317–1343.

Dixon, J. E., Stolper, E. M. & Holloway, J. R. (1995). An experimental study of water and carbon dioxide solubilities in mid ocean ridge basaltic liquids. 1. Calibration and solubility models. *Journal of Petrology* **36**, 1607–1631.

Drake, M. J. & Weill, D. F. (1975). Partition of Sr, Ba, Ca, Y, Eu^{2+}, Eu^{3+}, and other REE between plagioclase feldspar and magmatic liquid—experimental study. *Geochimica et Cosmochimica Acta* **39**, 689–712.

Gaetani, G. A. & Grove, T. L. (1998). The influence of water on melting of mantle peridotite. *Contributions to Mineralogy and Petrology* **131**, 323–346.

Gaetani, G. A., Grove, T. L. & Bryan, W. B. (1993). The influence of water on the petrogenesis of subduction-related igneous rocks. *Nature* **365**, 332–334.

Ghiorso, M. S. & Sack, R. O. (1995). Chemical mass-transfer in magmatic processes. 4. A revised and internally consistent thermodynamic model for the interpolation and extrapolation of liquid–solid equilibria in magmatic systems at elevated temperatures and pressures. *Contributions to Mineralogy and Petrology* **119**, 197–212.

Green, T. H. & Ringwood, A. E. (1968). Genesis of the calc-alkaline igneous rock suite. *Contributions to Mineralogy and Petrology* **18**, 105–162.

Grove, T. L. & Baker, M. B. (1984). Phase-equilibrium controls on the tholeiitic versus calc-alkaline differentiation trends. *Journal of Geophysical Research* **89**, 3253–3274.

Grove, T. L., Kinzler, R. J. & Bryan, W. B. (1993). Fractionation of mid-ocean ridge basalt (MORB). In: Phipps-Morgan, J. (ed.) *Mantle Flow and Melt Migration*. Geophysical Monograph 71, American Geophysical Union, Washington DC, pp. 281–311.

Grove, T. L., Donnelly Nolan, J. M. & Housh, T. (1997). Magmatic processes that generated the rhyolite of Glass Mountain, Medicine Lake volcano, N California. *Contributions to Mineralogy and Petrology* **127**, 205–223.

Grove, T. L., Elkins-Tanton, L. T., Parman, S. W., Chatterjee, N., Muntener, O. & Gaetani, G. A. (2003). Fractional crystallization and mantle-melting controls on calc-alkaline differentiation trends. *Contributions to Mineralogy and Petrology* **145**, 515–533.

Hamada, M. & Fujii, T. (2008). Experimental constraints on the effects of pressure and H_2O on the fractional crystallization of high-Mg island arc basalt. *Contributions to Mineralogy and Petrology* **155**, 767–790.

Housh, T. B. & Luhr, J. F. (1991). Plagioclase–melt equilibria in hydrous systems. *American Mineralogist* **76**, 477–492.

Kawamoto, T. (1996). Experimental constraints on differentiation and H_2O abundance of calc-alkaline magmas. *Earth and Planetary Science Letters* **144**, 577–589.

Kelemen, P. B., Hirth, G., Shimizu, N., Spiegelman, M. & Dick, H. J. B. (1997). A review of melt migration processes in the adiabatically upwelling mantle beneath oceanic spreading ridges. *Philosophical Transactions of the Royal Society, Series A* **355**, 283–318.

Kelley, K. A., Plank, T., Newman, S., Stolper, E., Grove, T. L., Parman, S. W. & Hauri, E. H. (2010). Mantle melting as a function of water content beneath the Mariana arc. *Journal of Petrology* **51**, 1711–1738.

Kent, A. J. R. & Elliott, T. R. (2002). Melt inclusions from Marianas arc lavas: implications for the composition and formation of island arc magmas. *Chemical Geology* **183**, 263–286.

Kushiro, I. (1974). Melting of hydrous upper mantle and possible generation of andesitic magma: an approach from synthetic systems. *Earth and Planetary Science Letters* **22**, 294–299.

Lee, J. & Stern, R. J. (1998). Glass inclusions in Mariana arc phenocrysts: A new perspective on magmatic evolution in a typical intra-oceanic arc. *Journal of Geology* **106**, 19–33.

Luhr, J. F. & Haldar, D. (2006). Barren Island Volcano (NE Indian Ocean): Island-arc high-alumina basalts produced by troctolite contamination. *Journal of Volcanology and Geothermal Research* **149**, 177–212.

Medard, E. & Grove, T. L. (2008). The effect of H_2O on the olivine liquidus of basaltic melts: experiments and thermodynamic models. *Contributions to Mineralogy and Petrology* **155**, 417–432.

Meen, J. K., Stern, R. J. & Bloomer, S. H. (1998). Evidence for magma mixing in the Mariana arc system. *Island Arc* **7**, 443–459.

Meijer, A. & Reagan, M. (1981). Petrology and geochemistry of the island of Sarigan in the Mariana Arc—calc-alkaline volcanism in an oceanic setting. *Contributions to Mineralogy and Petrology* **77**, 337–354.

Miller, M. S., Gorbatov, A. & Kennett, B. L. N. (2006). Three-dimensional visualization of a near-vertical slab tear beneath the southern Mariana arc. *Geochemistry, Geophysics, Geosystems* **7**, doi:10.1029/2005GC001110.

Miyashiro, A. (1974). Volcanic rock series in island arcs and active continental margins. *American Journal of Science* **274**, 321–355.

Newman, S., Stolper, E. & Stern, R. J. (2000). H_2O and CO_2 in magmas from the Mariana arc and back-arc systems. *Geochemistry, Geophysics, Geosystems* **1**, doi:1999GC000027.

Pearce, J. A., Stern, R. J., Bloomer, S. H. & Fryer, P. (2005). Geochemical mapping of the Mariana arc-basin system: Implications for the nature and distribution of subduction components. *Geochemistry, Geophysics, Geosystems* **6**, doi:10.1029/2004GC000895.

Pichavant, M. & Macdonald, R. (2007). Crystallization of primitive basaltic magmas at crustal pressures and genesis of the calc-alkaline igneous suite: experimental evidence from St Vincent, Lesser Antilles arc. *Contributions to Mineralogy and Petrology* **154**, 535–558.

Portnyagin, M., Almeev, R., Matveev, S. & Holtz, F. (2008). Experimental evidence for rapid water exchange between melt inclusions in olivine and host magma. *Earth and Planetary Science Letters* **272**, 541–552.

Roggensack, K. (2001). Unraveling the 1974 eruption of Fuego volcano (Guatemala) with small crystals and their young melt inclusions. *Geology* **29**, 911–914.

Shaw, A. M., Hauri, E. H., Fischer, T. P., Hilton, D. R. & Kelley, K. A. (2008). Hydrogen isotopes in Mariana arc melt inclusions: Implications for subduction dehydration and the deep-Earth water cycle. *Earth and Planetary Science Letters* **275**, 138–145.

Sisson, T. W. & Grove, T. L. (1993). Temperatures and H_2O contents of low-MgO high-alumina basalts. *Contributions to Mineralogy and Petrology* **113**, 167–184.

Spiegelman, M., Kelemen, P. B. & Aharonov, E. (2001). Causes and consequences of flow organization during melt transport: The reaction infiltration instability in compactible media. *Journal of Geophysical Research—Solid Earth* **106**, 2061–2077.

Stern, R. J., Fouch, M. J. & Klemperer, S. L. (2003). An overview of the Izu–Bonin–Mariana subduction factory. In: Eiler, J. M. (ed.) *Inside the Subduction Factory. Geophysical Monograph, American Geophysical Union* **138**, 175–222.

Stern, R. J., Kohut, E., Bloomer, S. H., Leybourne, M., Fouch, M. & Vervoort, J. (2006). Subduction factory processes beneath the Guguan cross-chain, Mariana Arc: no role for sediments, are serpentinites important? *Contributions to Mineralogy and Petrology* **151**, 202–221.

Tatsumi, Y. (1981). Melting experiments on a high-magnesian andesite. *Earth and Planetary Science Letters* **54**, 357–365.

Tatsumi, Y., Sakuyama, M., Fukuyama, H. & Kushiro, I. (1983). Generation of arc basalt magmas and thermal structure of the mantle wedge in subduction zones. *Journal of Geophysical Research* **88**, 5815–5825.

Wade, J. A., Plank, T., Stern, R. J., Tollstrup, D. L., Gill, J. B., O'Leary, J. C., Eiler, J. M., Moore, R. B., Woodhead, J. D., Trusdell, F., Fischer, T. P. & Hilton, D. R. (2005). The May 2003 eruption of Anatahan volcano, Mariana Islands: Geochemical evolution of a silicic island-arc volcano. *Journal of Volcanology and Geothermal Research* **146**, 139–170.

Wade, J. A., Plank, T., Melson, W. G., Soto, G. J. & Hauri, E. H. (2006). The volatile content of magmas from Arenal volcano, Costa Rica. *Journal of Volcanology and Geothermal Research* **157**, 94–120.

Walker, J. A., Roggensack, K., Patino, L. C., Cameron, B. I. & Matias, O. (2003). The water and trace element contents of melt inclusions across an active subduction zone. *Contributions to Mineralogy and Petrology* **146**, 62–77.

Wallace, P. J. (2005). Volatiles in subduction zone magmas: concentrations and fluxes based on melt inclusion and volcanic gas data. *Journal of Volcanology and Geothermal Research* **140**, 217–240.

Woodhead, J. D. (1988). The origin of geochemical variations in Mariana lavas—a general model for petrogenesis in intra-oceanic island arcs. *Journal of Petrology* **29**, 805–830.

Woodhead, J. D. (1989). Geochemistry of the Mariana Arc (Western Pacific)—source composition and processes. *Chemical Geology* **76**, 1–24.

Woodhead, J. D. (1990). The origin of geochemical variations in Mariana Lavas—a general model for petrogenesis in intraoceanic island arcs—Reply. *Journal of Petrology* **31**, 963–966.

Woodhead, J. D., Eggins, S. M. & Johnson, R. W. (1998). Magma genesis in the New Britain island arc: Further insights into melting and mass transfer processes. *Journal of Petrology* **39**, 1641–1668.